NeuroImage: Clinical 25 (2020) 102188

Contents lists available at ScienceDirect

NeuroImage: Clinical

journal homepage: www.elsevier.com/locate/ynicl

Reorganization of rich-clubs in functional brain networks during propofol-induced unconsciousness and natural sleep

Wang Shengpei[a,b,#], Li Yun[c,#], Qiu Shuang[a], Zhang Chuncheng[a], Wang Guyan[c], Xian Junfang[d], Tianzuo Li[c,e,$,**], He Huiguang[a,b,f,$,*]

[a] Research Center for Brain-inspired Intelligence and National Laboratory of Pattern Recognition, Institute of Automation, Chinese Academy of Sciences, Beijing, China
[b] University of Chinese Academy of Sciences, Beijing, China
[c] Department of Anesthesia, Beijing Tongren Hospital, Capital Medical University, Beijing, China
[d] Department of Radiology, Beijing Tongren Hospital, Capital Medical University, Beijing, China
[e] Beijing Shijitan Hospital, Capital Medical University, Beijing, China
[f] Center for Excellence in Brain Science and Intelligence Technology, Chinese Academy of Sciences, Beijing, China

ARTICLE INFO

Keywords:
Resting-state functional magnetic resonance images (rs-fMRI)
Brain network
Rich-club organization
Propofol-induced sedation
Natural sleep

Background: General anesthesia (GA) provides an invaluable experimental tool to understand the essential neural mechanisms underlying consciousness. Previous neuroimaging studies have shown the functional integration and segregation of brain functional networks during anesthetic-induced alteration of consciousness. However, the organization pattern of hubs in functional brain networks remains unclear. Moreover, comparisons with the well-characterized physiological unconsciousness can help us understand the neural mechanisms of anesthetic-induced unconsciousness.

Methods: Resting-state functional magnetic resonance imaging was performed during wakefulness, mild propofol-induced sedation (m-PIS), and deep PIS (d-PIS) with clinical unconsciousness on 8 healthy volunteers and wakefulness and natural sleep on 9 age- and sex-matched healthy volunteers. Large-scale functional brain networks of each volunteer were constructed based on 160 regions of interest. Then, rich-club organizations in brain functional networks and nodal properties (nodal strength and efficiency) were assessed and analyzed among the different states and groups.

Results: Rich-clubs in the functional brain networks were reorganized during alteration of consciousness induced by propofol. Firstly, rich-club nodes were switched from the posterior cingulate cortex (PCC), angular gyrus, and anterior and middle insula to the inferior parietal lobule (IPL), inferior parietal sulcus (IPS), and cerebellum. When sedation was deepened to unconsciousness, the rich-club nodes were switched to the occipital and angular gyrus. These results suggest that the rich-club nodes were switched among the high-order cognitive function networks (default mode network [DMN] and fronto-parietal network [FPN]), sensory networks (occipital network [ON]), and cerebellum network (CN) from consciousness (wakefulness) to propofol-induced unconsciousness. At the same time, compared with wakefulness, local connections were switched to rich-club connections during propofol-induced unconsciousness, suggesting a strengthening of the overall information commutation of networks. Nodal efficiency of the anterior and middle insula and ventral frontal cortex was significantly decreased. Additionally, from wakefulness to natural sleep, a similar pattern of rich-club reorganization with propofol-induced unconsciousness was observed: rich-club nodes were switched from the DMN (including precuneus and PCC) to the sensorimotor network (SMN, including part of the frontal and temporal gyrus). Compared with natural sleep, nodal efficiency of the insula, frontal gyrus, PCC, and cerebellum significantly decreased during propofol-induced unconsciousness.

Conclusions: Our study demonstrated that the rich-club reorganization in functional brain networks is characterized by switching of rich-club nodes between the high-order cognitive and sensory and motor networks

* Corresponding author at: Research Center for Brain-inspired Intelligence and National Laboratory of Pattern Recognition, Institute of Automation, Chinese Academy of Sciences, Zhongguancun East Rd. 95#, Beijing 100190, China
** Co-corresponding author at: Beijing Shijitan Hospital, Capital Medical University, No. 10 Tieyi Road, Yangfangdian Road, Haidian District, Beijing 100038, China.
E-mail addresses: trmzltz@126.com (T. Li), huiguang.he@ia.ac.cn (H. He).
# Both authors contributed equally to this work and should be considered co-first authors.
$ Both authors contributed equally to this work and should be considered Corresponding authors.

https://doi.org/10.1016/j.nicl.2020.102188
Received 18 June 2019; Received in revised form 31 December 2019; Accepted 18 January 2020
Available online 21 January 2020

during propofol-induced alteration of consciousness and natural sleep. These findings will help understand the common neurological mechanism of pharmacological and physiological unconsciousness.

1. Introduction

General anesthesia (GA) is a drug-induced, reversible condition, which comprises five behavioral states: hypnosis (loss of consciousness), amnesia, analgesia, immobility (no movement in response to pain stimuli), and hemodynamic stability with control of the stress response (Brown et al., 2010; Eikermann et al., 2011; Evers and Crowder, 2006; Purdon et al., 2009). However, mechanisms by which general anesthetics cause a reversible loss of consciousness have been a long-standing mystery (Franks, 2008). The neural activity in the central nervous system during anesthesia has been already characterized at the molecular and spinal levels. The γ-aminobutyric acid type A (GABA-A) and N-methyl-D-aspartate (NMDA) receptors appear to be the most important targets of anesthesia (Minert and Devor, 2016; Zecharia et al., 2009). Furthermore, the general anesthetics decrease the transmission of noxious information ascending from the spinal cord to the brain (Angel, 1993; Campagna et al., 2003; Collins et al., 1995). With the development of various neuroimaging techniques, the neural activity and functional connectivity (FC) patterns of the brain across different states of consciousness have been utilized to understand the mechanism of anesthetic-induced unconsciousness (MacDonald et al., 2015). Previous studies have suggested that the general anesthetics at a deep sedative dose preferentially reduced brain activation in higher-order information-processing regions but had no effect on the response of primary sensory cortices to stimuli (Alkire et al., 2008; Hudetz and Mashour, 2016). At the same time, connectivity studies suggested that under anesthesia, cortico-cortical connectivity reduced in higher-order brain networks, including the salience network (Guldenmund et al., 2013), the default-mode network (DMN) (Greicius et al., 2008; Jordan et al., 2013), and the executive control network (ECN) (Boveroux et al., 2010). Despite these recent advances, no consensus has been reached on the neurological mechanisms by which anesthetic drugs induce the loss of consciousness.

GA is thought to be a sleep-like behavioral state, such as amnesia, immobility, and reversible unconsciousness. Previous studies have suggested that both cases could involve the common mechanisms in loss of consciousness (Alkire et al., 2008; Franks and Zecharia, 2011). For example, connectivity studies of resting-state networks using functional magnetic resonance imaging (fMRI) have demonstrated that the alteration of cortico-cortical and thalamocortical connectivity patterns during sleep resembles that of the GA, induced by different drugs (Heine et al., 2012; Larson-Prior et al., 2009; Stamatakis et al., 2010). In particular, within-network and between-network functional disconnections were found in the DMN and frontal–parietal network (FPN). Moreover, connections between DMN, FPN, primary sensors, and thalamocortical sensors were maintained during unconsciousness (both in natural sleep and GA). In contrast, some other studies have suggested that anesthetic-induced unconsciousness is mediated by a different mechanism than that for sleep. For example, propofol-induced unconsciousness was found to be associated with preserved DMN connectivity in the posterior cingulate gyrus/precuneus; while, during natural sleep state, ECN connectivity with the bilateral superior parietal lobules was preserved compared with propofol- and dexmedetomidine-induced unconsciousness (Guldenmund et al., 2017). Certainly, the hypothesis that GA and sleep share brain mechanisms still need more confirmation and detailed investigation. Nonetheless, its comparisons with the features of natural sleep could help us understand how anesthetics work and the neuronal circuits the anesthetics affect (Franks, 2008; Franks and Zecharia, 2011).

Propofol is one of the most commonly used hypnotics agents that reversibly induce a state of unconsciousness (Brown et al., 2010). The neurological mechanism of propofol-induced anesthesia has always been a major focus (Lee, 2012; Short and Bufalari, 1999). Recently, some studies have indicated that PIS is associated with regional hypometabolism in a widespread cortical network; the metabolism of bilateral frontal and parietal associative regions was encompassed, while that of sensory and motor cortices was relatively preserved (Alkire and Miller, 2005; Baars et al., 2003; Zalucki and van Swinderen, 2016). Meanwhile, some anesthesia studies focused on the posterior cingulate cortex (PCC)/ precuneus and have shown the alteration of the connectivity pattern induced by propofol (Guldenmund et al., 2016; Liu et al., 2013; Stamatakis et al., 2010). More recent studies indicated that the higher-order, resting-state networks, such as the external control and salience networks, were involved in the alteration of consciousness (Boveroux et al., 2010; Guldenmund et al., 2013; Liu et al., 2012). There is great progress in understanding how propofol acts on the corticocortical connectivity of functional networks; however, the mechanism of propofol-induced sedation, its similarities, and differences with the natural sleep remain unclear.

Graph theoretical network analysis has been widely used to study the functional architecture of the brain (Huang et al., 2018a; Pappas et al., 2019; Schröter et al., 2012). A ubiquitous feature of network organization is the existence of highly connected nodes, which often hold privileged positions of functional importance but are also points of vulnerability, as attacks targeting these nodes will lead to the rapid disintegration of the system as a whole (Albert et al., 2000; Barabasi and Albert, 1999; Holme et al., 2002; Piece, 1965; Vértes et al., 2014). These have been termed rich-clubs, which are elite cliques of high-degree network hubs that are connected topologically with high efficiency (i.e., short path length between any pair of rich-club nodes) (Towlson et al., 2013). Many complex systems can be partitioned into a small rich-club and a large poor periphery. The rich-club usually plays a central role in the static and dynamic processes of the complex systems and is important for the overall function of the network (Colizza et al., 2006; Towlson et al., 2013). Therefore, significant attention has been paid to the prominent effects of the richest elements and their organization (Csigi et al., 2017; Xu et al., 2010). Previous studies based on neuroanatomically informed network architectures have highlighted the important role of rich-clubs, which are disrupted or reconfigured after exposure to different general anesthetics (i.e., propofol, sevoflurane, and ketamine) (Bonhomme et al., 2016; Lee et al., 2013; Mashour and Hudetz, 2018; Moon et al., 2015; Schröter et al., 2012). Based on these studies, we hypothesized that (i) the rich-clubs reorganize in the functional brain network from consciousness to unconsciousness induced by propofol; and (ii) the alteration of rich-club regions may be mainly distributed in high-order cognitive networks. To test these hypotheses, we constructed large-scale functional brain networks based on fMRI during pharmacological unconsciousness (including wakefulness, mild propofol-induced sedation [m-PIS] and deep PIS [d-PIS]) and physiological unconsciousness (including wakefulness and natural sleep). Then, based on the graph theory, rich-club organization and nodal properties (nodal strength and efficiency) of the brain network were assessed and analyzed across PIS and natural sleep.

2. Materials and methods

2.1. Participants

The study was approved by the Institutional Review Board of

Beijing Tong Ren Hospital affiliated to Capital Medical University. All subjects gave written informed consent before joining the study.

Initially, 24 right-handed and healthy volunteers were recruited to participate in the study from December 1, 2015, to November 30, 2016. Twelve participants who could easily fall asleep were assigned to the sleep group, and another12 participants were included in the PIS group: 6 males (M) and 6 females (F) in both groups. According to the physical examination and mental evaluation by Wechsler Adult Intelligence Scale-Revised China (WAIS-RC), all subjects were assessed for both physical and psychiatric health. All subjects were fit and well (BMI < 30, American Society of Anesthesiology grade I). Subjects with the following conditions were excluded: (i) a history of allergy, head trauma or surgery, drug addiction, asthma, motion sickness, or previous problems during anesthesia; (ii) a contraindication to MRI examination, such as vascular clips or metallic implants, dental filling, or claustrophobia; (iii) the females in menstrual periods and menopause. Finally, the dataset utilized in our study is a subset of the initial dataset and is identical to the data used in our previous study (Li et al., 2018)., including 8 participants in the PIS group (4 M/4F; mean age ± SD: 24.5 ± 5.2 y) and 9 participants (4M5 F, mean age ± SD: 23.5 ± 3.8 y) in the sleep group. The exclusion criteria included: (i) a dysphoric reaction to propofol causing great body movement; (ii) 3.0 mm and 3.0° in max head motion in the preprocessing step. Detailed demographics for all participants are listed in Table 1. Additionally, before the data acquisition, participants in the PIS group followed the standard pre-anesthesia fasting regimen with fluid restrictions. Upon completion of the experiment, the subjects were discharged after full recovery (Post-Anesthetic Discharge Scoring System scoring > 9).

2.2. Experimental protocol

The experimental protocol was described in detail in our previous study (Li et al., 2018). All participants were scanned in wakefulness, in a relaxed state with eyes closed. Participants in the PIS group were intravenously injected with 1% propofol (Diprivan, AstraZeneca UK Limited) through a target-controlled infusion pump (Graseby 3500 pump, Smiths Medical International Ltd.) programmed with the Marsh model (Absalom et al., 2009; Adapa et al., 2012; Marsh et al., 1991). The target effect-site concentrations (Ce) were set to 0.5–2.0 μg/ml with a 0.5 μg/ml interval. When the pre-setting concentrations were reached, a 5-min pause was allowed for equilibration, and the fMRI data were acquired for a total scanning time of 400 s. Meanwhile, sedation states were evaluated by the Ramsay Sedation Scale (RSS) (Namigar et al., 2017; Ramsay et al., 1974; Stamatakis et al., 2010). When the RSS score reached 3 or 4, the subjects were considered to reach the m-PIS state. When the RSS score reached 5 or 6, they were considered to reach the D-PIS state. Meanwhile, for all subjects, physiological parameters including heart rate (HR), oxyhemoglobin saturation (SpO_2), mean arterial pressure (MAP), and end-tidal carbon dioxide ($PetCO_2$) were continuously recorded during the entire procedure. Importantly, there was no significant difference for HR, SpO_2, and $PetCO_2$ among wakefulness, m-PIS, and D-PIS, while MAP was significantly decreased during D-PIS compared with wakefulness and m-PIS. Accordingly, we considered the MAP parameter as a covariate of no interest in statistical analysis for the rich-club organization. The details of the physiological parameters are shown in Table 1. Two dedicated veteran anesthesiologists were responsible for the administration of propofol and monitoring of physiological status during the entire session.

Participants in the sleep group were not injected with any drug or suspension. All subjects spontaneously fell asleep under the scanner. Meanwhile, MRI-compatible electroencephalogram (EEG) (MP150, BIOPAC Systems, Inc.) signals were acquired to evaluate the stage of sleep. A special EEG expert determined the sleep stage for this study. Importantly, the fMRI data during the non-rapid-eye-movement (NREM) sleep stage 2 (N2) were extracted and analyzed. The EEG analysis for sleep stage identification was provided in Supplementary material, which is the same as in our prior study (Li et al., 2018).

2.3. Data acquisition

The fMRI data acquisition consisted of resting-state fMRI volumes in three states in the PIS group (wakefulness, m-PIS, and D-PIS) and two states in the sleep group (wakefulness and sleep). Functional images were acquired using a GE Signa HDxt 3.0T MRI scanner (General Electric Medical Systems, Milwaukee, WI, USA) at the Tong Ren Hospital. For each subject, a high-resolution structural image was acquired by a three-dimensional MRI sequence using an axial fast spoiled gradient recalled sequence (FSGPR) with the following parameters: repetition time (TR) = 8.876 ms, echo time (TE) = 3.516 ms, flip angle (FA) = 13°, data matrix = 256 × 256, and field of view (FOA) = 256 mm × 256 mm with 196 continuous sagittal slices of 1-mm thickness. The functional images were obtained with an echo-planer imaging (EPI) sequence with the following parameters: TR = 2000 ms, TE = 35 ms, FA = 90°, data matrix = 64 × 64, resolution = 3.75 × 3.75 mm, and slices thickness = 5 mm with an inter-slice gap of 1 mm. For each subject, a total of 200 volumes with 28 axial slices were acquired, resulting in a total scan time of 400 s. All participants were fixed to avoid head or body motion in the state of unconsciousness (natural sleep and PIS states).

2.4. Data preprocessing

The preprocessing was operated using statistical parametric mapping (SPM) (SPM8, http://www.fil.ion.ucl.ac.uk/spm/) and data processing & analysis for brain imaging (resting-state) (DPABI, http://www.rfmri.org/dpabi) (Yan et al., 2016). Firstly, the first 10 volumes in the time series were excluded to avoid nonequilibrium effects in the MR

Table 1
Demographic and clinical details of the participants.

	Propofol-induced sedation Wakefulness	m-PIS	d-PIS	Natural sleep Sleep
Number of Subjects		8		9
Gender (M/F)		4 M / 4F		4 M / 5F
Age (Mean ± SD)		24.5 ± 5.2		23.5 ± 3.8
Ramsay Sedation Scale	\	3–4	5–6	/
Physiological Parameters				
HR (bpm)	64.6 ± 13.48	59.7 ± 11.12	59.83 ± 13.69	/
SpO_2(%)	97.8 ± 0.75	97.6 ± 0.49	96.97 ± 0.70	/
MAP (mmHg)*	81.73 ± 8.90	72.03 ± 6.30	62.26 ± 7.96	/
$PetCO_2$ (mmHg)	40.2 ± 2.63	40.8 ± 2.93	41.13 ± 3.51	/

PIS: propofol induced sedation; m-PIS: mild PIS; D-PIS: deep PIS;
HR, heart rate; SpO_2, oxyhemoglobin saturation; MAP, mean arterial pressure; $PetCO_2$, end-tidal carbon dioxide;
* represents the significant difference with repeated measured ANOVA among wakefulness, m-PIS and D-PIS in PIS group.

signal, and the functional images were corrected for the slice-timing by interpolating the voxel time using slice interpolation. Next, all functional images were spatially realigned for head movement correction and co-registered to their corresponding anatomical images. The resulting images were then spatially normalized to the Montreal Neurological Institute space and resampled to 3 × 3 × 3 mm^3 voxels (Feindel, 1991). The spatial smoothing was performed using a Gaussian kernel with 6 mm full-width at half maximum The following band-pass temporal filtering with a 0.01–0.10 Hz cutoff was used to minimize the physiological noise of high-frequency components because previous studies have indicated that network fluctuation is maximally observed at low frequencies (Boyacioglu et al., 2013; Gohel and Biswal, 2015; Niazy et al., 2011). Although the emerging evidence has demonstrated that spontaneous activities may persist in higher frequency bands (above 0.1 Hz) (Chen and Glover, 2015; Cordes et al., 2001; Craig et al., 2018), mechanisms underlying the present observations were not yet conclusive (Chen and Glover, 2015). Hence, the typical frequency range (0.01 – 0.10 Hz) was adopted in our study. Finally, the potential sources of 24 head motion parameters, global signals (GS), white matter signals, and cerebrospinal fluid signals were regressed out to remove their effects. In particular, the 24-movement parameter included the 6-current and 6-past position parameters, along with the square of each current and past parameter (Friston et al., 1996; Yan et al., 2013).

Given a possible confounding effect of micro-movements on functional connectivity (van Dijk et al., 2012), the framewise displacement (FD) values were calculated for each subject using the Jenkinson formula, which reflects the temporal derivative of the movement parameters (Power et al., 2012; Yang et al., 2014). The subjects who had mean FD > 0.5 mm, translation > 3 mm, or rotation > 3° were excluded. The remaining 8 participants (4 M/4F) in the PIS group and 9 participants (4 M/5F) in the sleep group were included for further analysis.

GS regression (GSR) is one of the most debated preprocessing strategies for resting-state fMRI (Li et al., 2019; Murphy and Fox, 2017). GSR may increase tissue sensitivity, decrease motion dependency, and enhance the overall neuronal-hemodynamic correspondence (Fox et al., 2009; Keller et al., 2013; Satterthwaite et al., 2013; Yan et al., 2013); however, it also alters the inter-individual differences at the group level (Gotts et al., 2013; Saad et al., 2012; Xu et al., 2018). More importantly, the GS is related to neural activity (Schölvinck et al., 2010) and exhibits a significant negative correlation with EEG measures of vigilance across the subjects (Wong et al., 2013). To date, the consensus has not been reached on the standards for the use of GSR (Xu et al., 2018). One of the recent studies with propofol has shown that upon the application of GSR, there were more functional brain networks observed with significant task modulation of temporal variability during wakefulness compared with that without GSR (Huang et al., 2018b). These improvements may be resulting from the fact that GSR can further remove nonneuronal sources of global variance such as respiration and movement. For these reasons, GSR was also performed in our study.

2.5. Functional brain networks construction

The functional brain network for each subject was constructed firstly according to the Dos-160 template, including 160 regions of interest (ROIs) (Fig. 1) (Dosenbach et al., 2010). The template was regarded as the optimal template for constructing functional brain networks (Wang et al., 2016; Yao et al., 2015) and has been applied in numerous brain imaging studies and integrated into several brain network toolboxes (Cao et al., 2014; Choe et al., 2017; Wang et al., 2015; Xia et al., 2013). Additionally, a recent study used this template to integrate the rich-club organization of functional brain networks (Wang et al., 2016). The 160 ROIs were assigned to 6 functional brain subnetworks, which included the default mode network (DMN), the fronto-parietal network (FPN), cingulo-opercular network (CON), sensorimotor network (SMN), occipital network (ON), and cerebellum network (CN) (Wang et al., 2016; Yao et al., 2015). Firstly, for each subject, the mean BOLD signal time series from the 160 ROIs (spherical

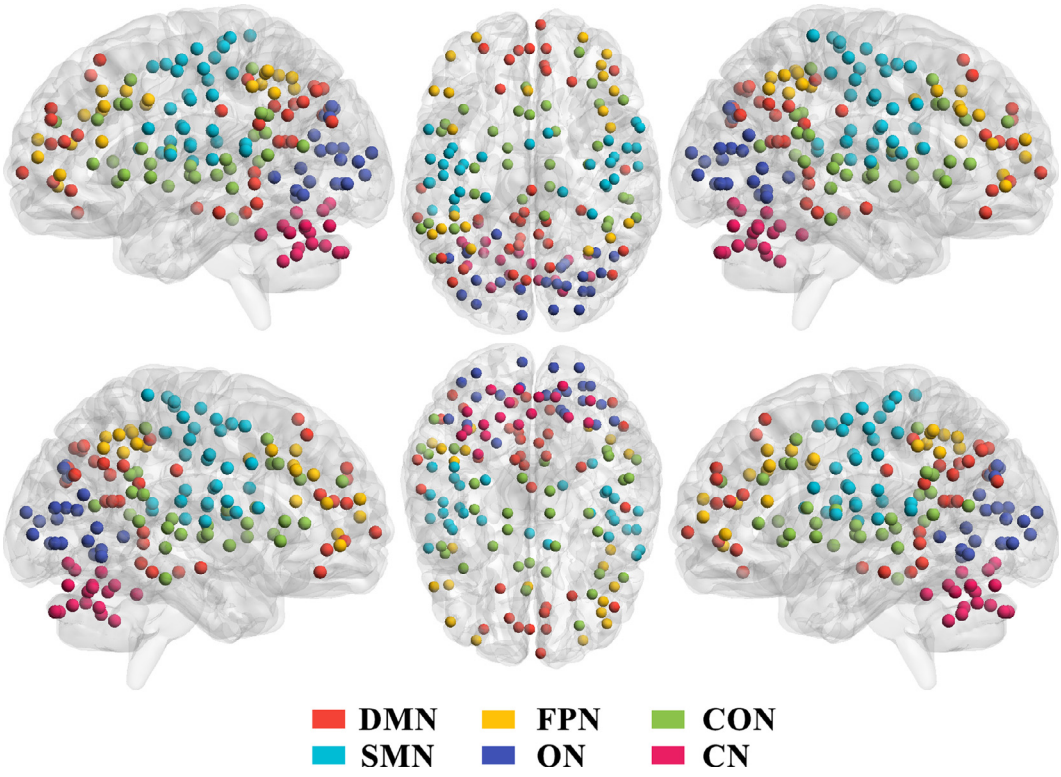

Fig. 1. The regions of interest (ROIs) in the Dos-160 template. The different colors represented different brain functional networks. DMN: the default mode network, FPN: the fronto-parietal network, CON: the cingulo-opercular network, SMN: the sensorimotor network, ON: the occipital network, CN: the cerebellum network.(For interpretation of the references to colour in this figure legend, the reader is referred to the web version of this article.)

radius of 5 mm) were extracted by averaging the time courses of all the voxels within the ROIs. Next, Pearson's linear correlation was calculated between the mean time series of each ROI. Then, a 160*160 symmetric correlation matrix was constructed and the Fisher-z transformation was applied to the symmetric correlation matric. Moreover, because of the present ambiguity regarding the meaning of negative correlation (Chai et al., 2012; Murphy et al., 2008; Schölvinck et al., 2010), the absolute value matrix was calculated in our

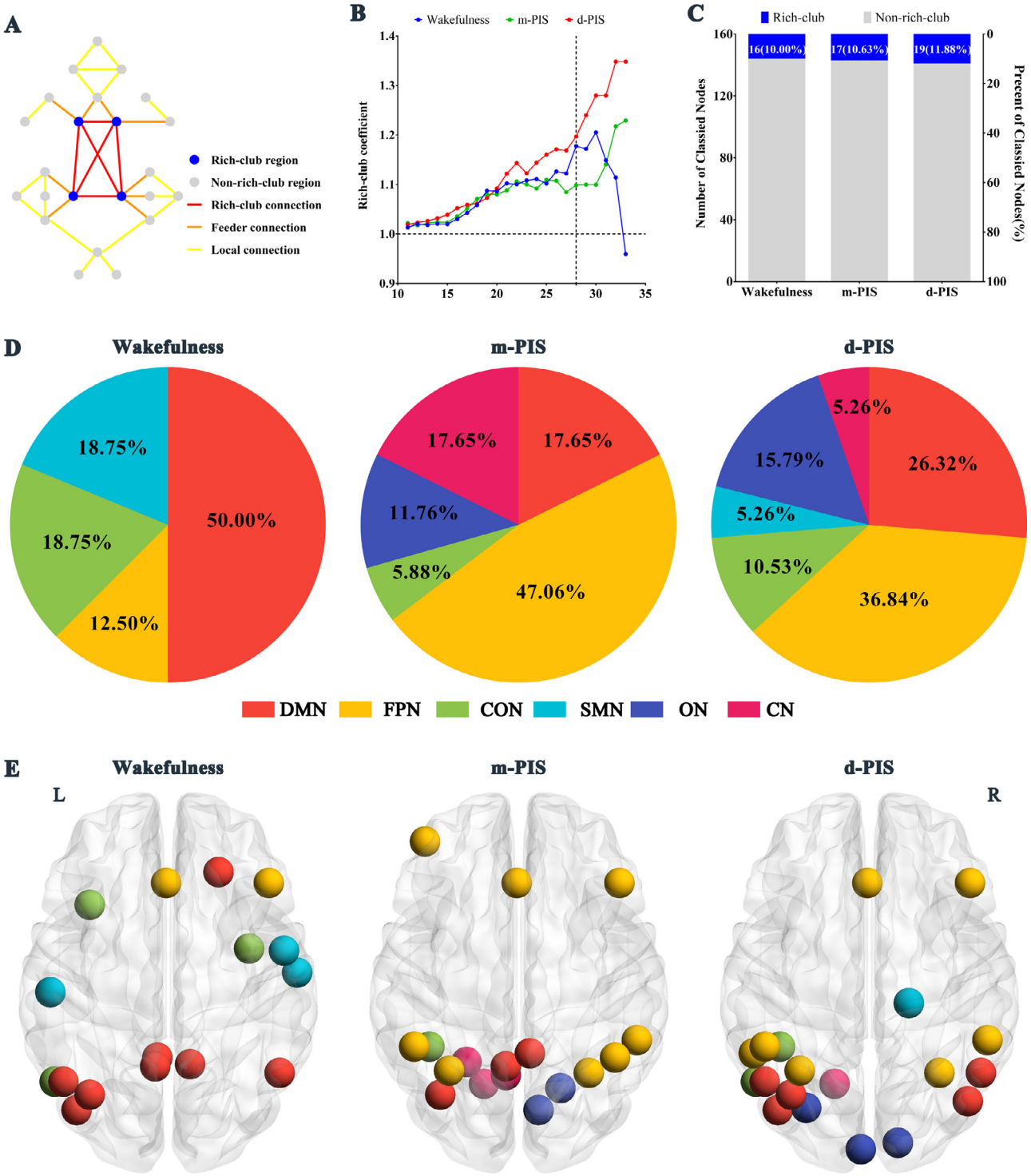

Fig. 2. The rich-club organization and the distribution of rich-club regions of the PIS group. (A) Schematic diagram of a network with high-degree rich-club nodes (blue) that are also highly connected among one another. The connection among rich-club nodes is so-called rich-club connections (red), while connections linking rich-club nodes to non-rich-club nodes are labeled feeder connections (orange) and connections among non-rich-club nodes are local connections (yellow). (B) Rich-club coefficients normalized relative to random are shown in blue (wakefulness), green (m-PIS), red (d-PIS). The coefficients are plotted against degree, between 11 and 35. (C) Number and percent of rich-club regions during wakefulness (left), m-PIS (middle) and D-PIS (right). (D) The percent of rich-club regions in the different functional brain networks during wakefulness (left), m-PIS (middle) and D-PIS (right). (E) The distribution of rich-club regions in the whole brain network during wakefulness (left), m-PIS (middle) and D-PIS (right). The different colors represented different brain functional networks.(For interpretation of the references to colour in this figure legend, the reader is referred to the web version of this article.)

study, and the diagonal values were set to zeros. Finally, the connectivity matrices were threshold by cost (i.e., connection density) following the previous graph-based study of the brain network (Wen et al., 2017). Our study investigated the different costs: 10%, 12%, 15%, and 20%. The cost of 10% was reported in the main text and results for other costs (12%, 15%, and 20%) were presented in the Supplementary material to ensure that the results did not depend solely on one cost.

2.6. Rich-club analysis

2.6.1. Rich-club organization

Rich-club organization based on the group-averaged network can be analyzed in either unweighted or weighted functional networks. In our study, the weighted networks were adopted to analyze the rich-club organization alteration between propofol-induced sedation and natural sleep. The weighted network nodes were defined as 90 ROIs based on the Dos-160 atlas and these nodes were linked by edges with weights denoting function connectivity between the two regions. For a weighted network, the rich-club nodes were defined according to the group-averaged weighted network in the following steps. Firstly, all FCs of the network were ranked according to the connectivity weight, resulting in a vector W^{ranked}. The degree (k) of each node was computed as the number of links to other nodes in the network. Next, for each value of k, we selected the set of nodes with a degree larger than k, counted the number of links $E > k$, and computed their collective weight $W > k$ as the sum of the weights of the resulting $E > k$ connections. The weighted rich-club parameter $\phi^w(k)$ was defined as the ratio between $W > k$ and the sum of the weights of the strongest $E > k$ connections, given by the top $E > k$ number of connections of the ranked connections in W^{ranked}. That is, $\phi^w(k)$ is given by

$$\phi^w(k) = = \frac{W_{>k}}{\sum_{l=1}^{E_{>k}} w_l^{ranked}} \tag{1}$$

Based on each weighted network, we formed $l =$ 1,000 random networks by keeping the original weights and degrees. From each of the randomized networks, for each level of k, we estimated the rich-club coefficient $\phi_{norm}^w(k)$. Furthermore, we computed the mean $\phi_{norm}(k)$ by averaging the rich-club coefficients across all the random networks. The normalized rich-club coefficient $\phi_{norm}^w(k)$ is given by (Rubinov and Sporns, 2010; van den Heuvel and Sporns, 2011):

$$\phi_{norm}^w(k) = \frac{\phi^w(k)}{\phi_{random}(k)} \tag{2}$$

Previous studies have shown that the weighted network had a rich-club organization for $\phi_{norm}^w(k) > 1$ over a continuous range of ks (Rubinov and Sporns, 2010; van den Heuvel and Sporns, 2011).

2.7. Classification of nodes and connections

Group of rich-club members was selected based on a group-averaged and sparse network, averaging the individual weighted brain functional networks across the group of participants (van den Heuvel and Sporns, 2011). As was the case for small-world and scale-free organization (Rubinov and Sporns, 2010), the presence of rich-club organizations should be regarded as a topological property of the network as a whole, with the rich-club organization associated with a range of degrees k when $\phi_{norm}(k)$ exceeds 1.

Rich-club selection allowed for the classification of the edges of the network into three connection classes; “rich-club” connections (linking the rich-club members), “feeder connections” (linking rich-club nodes to non-rich-club nodes), and “local connections” (describing the network connections that linked the non-rich-club nodes) (van den Heuvel and Sporns, 2011). Fig. 2A provides a schematic illustration of the two classes of nodes and three classes of connections.

2.8. Nodal properties analysis

To further explore the importance of rich-club regions, nodal properties i.e. nodal strength and nodal efficiency were calculated and analyzed. They are defined as follows (Watts and Strogatz, 1998):

Nodal strength (NS) is the sum of the edge weights of all the connections of a node:

$$NS_i = \sum_{j \in N} W_{ij} \tag{3}$$

Where, W_{ij} is the edge weight between node i and node j. It quantifies whether a node is relevant to the graph.

Nodal efficiency (NE) is the inverse of the characteristic path length between the pair of nodes:

$$NE_i = \frac{1}{N-1} \sum_{j \neq i \in G} \frac{1}{L_{ij}} \tag{4}$$

Where, L_{ij} is the weighted characteristic path length between nodes i and j.

2.9. Statistical analysis

Differences of rich-club organization and nodal properties (nodal strength and efficiency) among different states in the PIS group and sleep group were tested using three different methods: (i) one-way repeated measured analysis of variance (ANOVA) for the whole process of sedation (including wakefulness, m-PIS, and D-PIS) in the PIS group and a paired two-tailed t-test as an orthogonal analysis to find differences between the different states, (ii) a two-tailed paired t-test to probe the differences between wakefulness and sleep states in the sleep group, (iii) a two-tailed two-sample t-test to determine the significant alteration between the mild/deep sedation and natural sleep. Additionally, three parameters including age, gender, and MAP were considered as covariates of no interest and regressed out to avoid their effects. Finally, all p values less than 0.05 and the false discovery rate (FDR) correction was set to determine the significance level.

3. Results

3.1. Rich-club analysis in propofol-induced sedation group

3.1.1. Rich-club organization in functional brain networks

The relevant rich-club parameters were calculated to quantify the rich-club organization of the network from consciousness to unconsciousness induced by propofol. The group-averaged functional network during wakefulness, m-PIS, and D-PIS states revealed the rich-club organization. The rich-club coefficient curves (R_{norm}) of the different states are presented in Fig. 2B. Compared with the wakefulness and m-PIS states, the rich-club parameter (k $\leq$ 25) increased in the D-PIS state. Rich-club parameters (25 $\leq$ k $\leq$ 30) in the m-PIS state slightly decreased compared with the wakefulness state. Furthermore, as is the case of small-world and scale-free organization, the presence of rich-club organization should be regarded as a topological property of the network, with the rich-club organization associated with a range of degrees k with R_{norm} exceed 1. Previous studies have shown consistent results when examining rich-clubs across different selection thresholds (Harriger et al., 2012; Reus and van den Heuvel, 2013; van den Heuvel and Sporns, 2013, 2011). In our study, we chose the degree (k = 28) to explore the alteration of rich-club regions and connections from consciousness to unconsciousness induced by propofol. The rich-club organization for the different degree levels in the PIS group is shown in Supplementary Figure 1.

3.2. Distribution of rich-club regions during propofol-induced sedation

The rich-club regions were selected on a group level, as described in several previous studies (Ball et al., 2014; Daianu et al., 2015; Li et al., 2017; Zhao et al., 2017). The number and percentage of rich-club regions at the $k = 28$ level in three different states are shown in Fig. 2C. The percent of rich-club nodes across the different states did not show any remarkable change (wakefulness: 16 rich-club nodes, 10.00%; m-PIS: 17, 10.6%; D-PIS: 19, 11.88%), which indicated that the number of rich-club nodes was consistent during the whole process of sedation induced by propofol. However, the distribution of rich-club regions in brain intrinsic networks was different among the different states. As shown in Fig. 2D, the main rich-club nodes in the wakefulness state were distributed in the DMN (50%), FPN (12.50%), CON (18.75%), and SMN (18.75%), with none of the rich-club nodes in the ON and CN. The main rich-club nodes in the m-PIS state were distributed uniformly in the DMN (17.65%), FPN (47.06%), CON (5.88%), ON (11.76%), and CN (17.65%), and none of the rich-club nodes were observed in the SMN network. All rich-club nodes in the D-PIS were located in the DMN (26.32%), and others were uniformly distributed in the FPN (36.84%), CON (10.53%), SMN (5.26%), ON (15.79%), and CN (5.26%). These results suggested that the rich-club regions were reorganized from consciousness to unconsciousness induced by propofol. Particularly, a part of the rich-club regions was switched between high-order cognitive systems network (DMN and FPN) and sensory systems (SMN and ON).

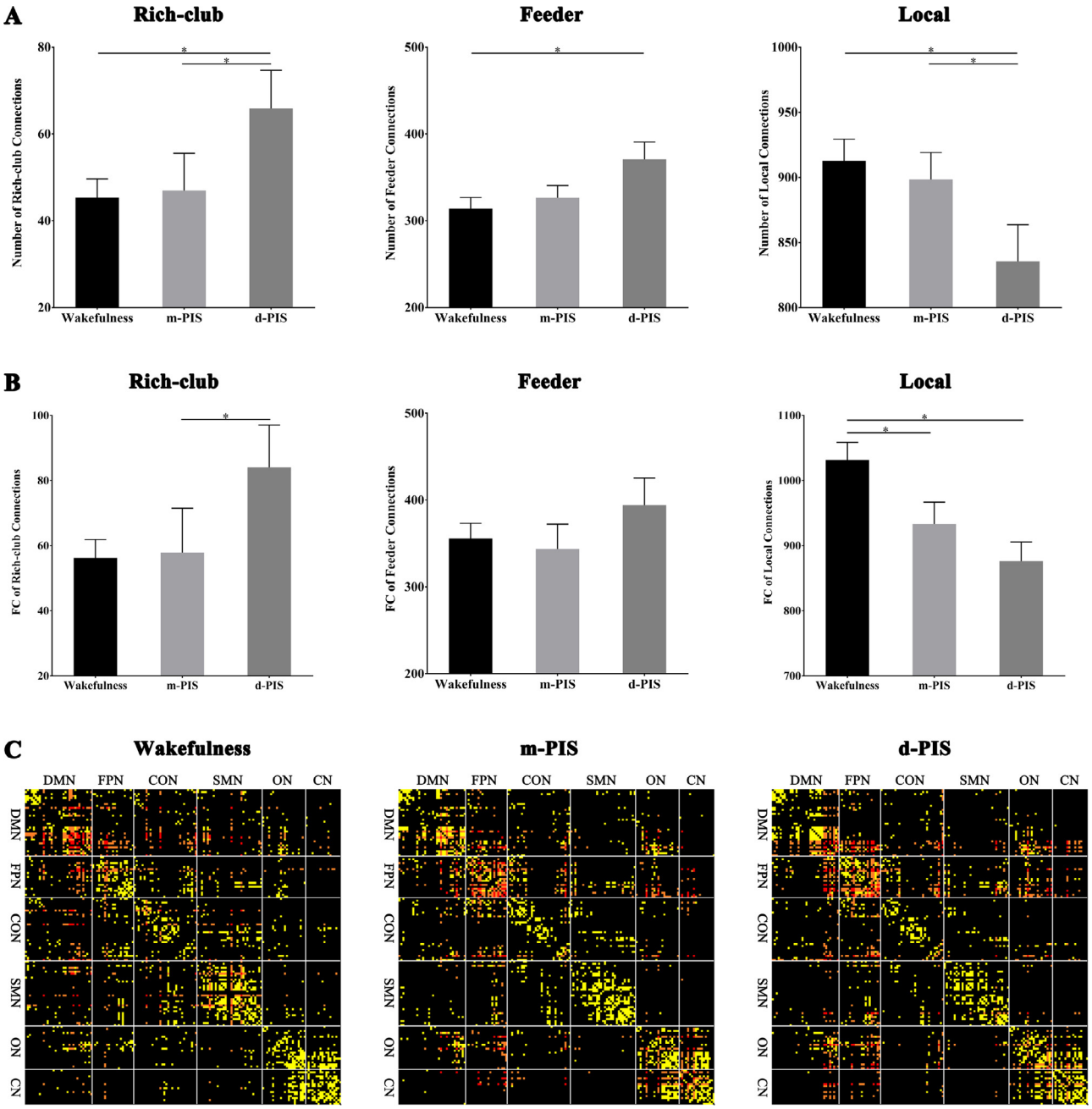

Fig. 3. The significant alteration in the number and strength of different categories of connections in the PIS group. (A) The significant alteration in the number of rich-club (left), feeder (middle) and local (right) connections. * represented the significant difference between the different states ($p < 0.05$). Error bar represented a standard error of mean (SEM). (B) The significant alteration in the strength of rich-club (left), feeder (middle) and local (right) connections. (C) The distribution of different categories of connections in the group-averaged functional brain network during wakefulness (left), m-PIS (middle) and D-PIS (right). The different colors represented the different categories of connections (red: rich-club connection; orange: feeder connection; yellow: local connection).(For interpretation of the references to colour in this figure legend, the reader is referred to the web version of this article.)

To further explore the reorganization of rich-clubs, the transformation of detailed rich-club regions was examined. As shown in Fig. 2E, in the wakefulness state, most of these rich-club nodes were located in the bilateral angular gyrus, anterior insula, middle insula, bilateral post cingulate cortex (PCC), precentral gyrus, precuneus, dorsal prefrontal cortex (dPFC), superior frontal cortex, inferior parietal lobe (IPL), and temporal gyrus. However, in both m-PIS and D-PIS states, the majority of the rich-club nodes were located in the anterior cingulate cortex (ACC), inferior parietal lobe (IPL), inferior parietal sulcus (IPS), dorsal prefrontal cortex, and medial cerebellum. Furthermore, a part of the rich-club nodes including the precuneus, lateral and medial cerebellum, and occipital was present only in the m-PIS, whereas, rich-club nodes including angular and posterior occipital gyrus were present only in the D-PIS state. Additionally, we found the results of robustness for the costs

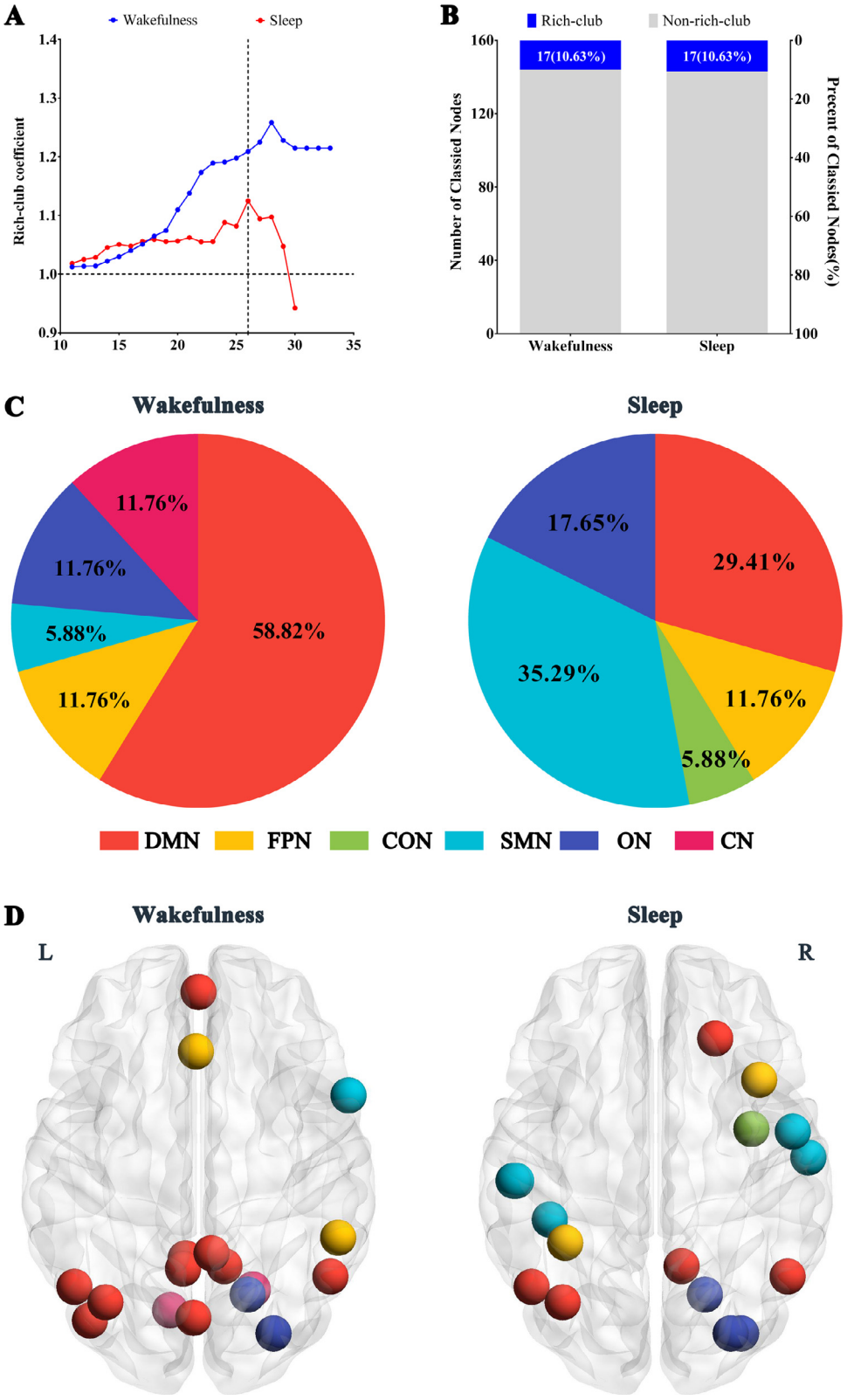

Fig. 4. The rich-club organization and the distribution of rich-club regions in the sleep group. (A) Rich-club coefficients normalized relative to random are shown in blue (wakefulness), red (sleep). The coefficients were plotted against degree, between 11 and 35. (B) Number and percent of rich-club regions during wakefulness (left) and sleep (right). (C) The percent of rich-club regions in the different functional brain networks during wakefulness (left) and sleep (right). (D) The distribution of rich-club regions in the whole brain network during wakefulness (left) and sleep (right). The different colors represented different brain functional networks.(For interpretation of the references to colour in this figure legend, the reader is referred to the web version of this article.)

of 12%, 15%, and 18% (Supplementary Figure 2 - 4). The above results suggested that the rich-club regions in the wakefulness state, including the superior frontal, post cingulate cortex, and anterior and middle insula were the first to be affected by propofol. As the depth of sedation subsequently increased to unconsciousness, the rich-club regions, including the ventral anterior prefrontal cortex, precuneus, and part of the anterior and middle occipital cortex, follow. Moreover, during unconsciousness induced by propofol, the rich-club regions, including the medial cerebellum, inferior parietal lobe, and sulcus (IPL and IPS) were found to play a crucial role.

3.3. The density of rich-club, feeder and local connections

On the basis of the categorization of the brain regions in rich-club and non-rich-club regions, network connections can be classified into

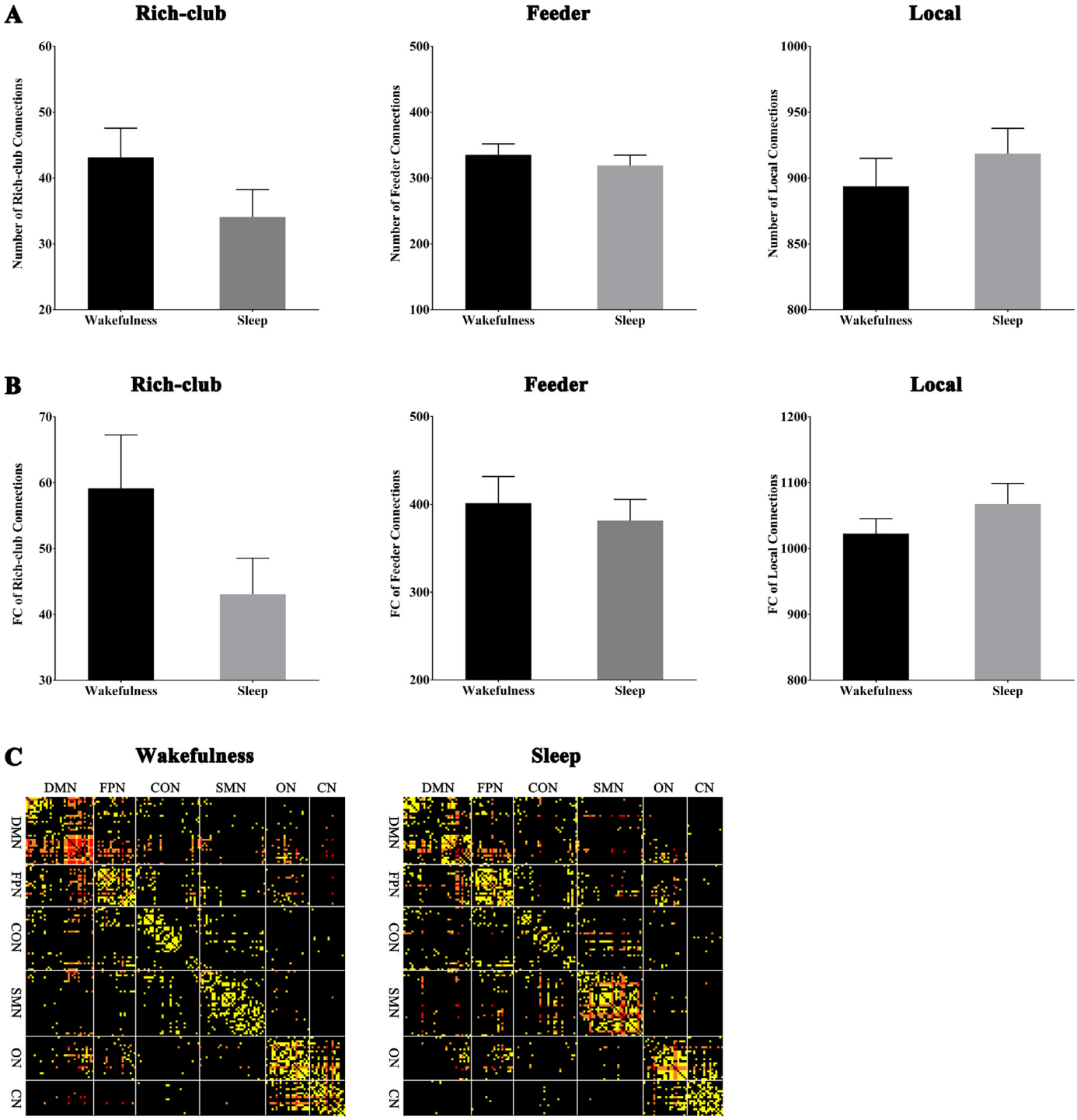

Fig. 5. The significant alteration in the number and strength of different categories of connections in the sleep group. (A) The significant alteration in the number of rich-club (left), feeder (middle) and local (right) connections. * represented the significant difference between the different states ($p < 0.05$). Error bar represented SEM. (B) The significant alteration in the strength of rich-club (left), feeder (middle) and local (right) connections. (C) The distribution of different categories of connections in the group-averaged functional brain network during wakefulness (left) and sleep (right). The different colors represented the different categories of connections (red represented rich-club connection; orange: feeder connection; yellow: local connection).(For interpretation of the references to colour in this figure legend, the reader is referred to the web version of this article.)

three topological categories: rich-club connection, feeder connection, and local connection (Fig. 2A). The number of three categories of connections with respect to different states were significantly altered (repeated measurements of ANOVA, rich-club, $F = 4.1160$; $p = 0.0393$; feeder: $F = 4.1073$, $p = 0.0395$; local: $F = 4.3986$, $p = 0.0329$). The details are shown in Fig. 3A. Compared with the wakefulness, the number of rich-club and feeder connections significantly increased during the D-PIS (two-tail paired *t*-test, rich-club: $T = 2.5118$, $p = 0.0403$; feeder: $T = 2.4326$, $p = 0.0452$) and the number of local connections significantly decreased ($T = -2.5061$, $p = 0.0406$). The number of rich-club connections in the D-PIS state was significantly larger than that in the m-PIS state ($T = 2.3852$, $p = 0.0485$). Moreover, the strength of local connections showed similar results ($F = 10.2768$, $p = 0.0018$). The details are shown in Fig. 3B. Compared to the wakefulness state, the strength of local connections was significantly lower in the m-PIS ($T = -2.3638$, $p = 0.0500$) and D-PIS states ($T = -4.5517$, $p = 0.0026$). Additionally, the strength of rich-club connections in the D-PIS state was significantly increased compared with that in the m-PIS state ($T = -2.3942$, $p = 0.0479$). These results suggest that local connections tended to be switched to rich-club connections during unconsciousness induced by propofol and the communications of the intra-rich-club organization as well as the between-rich-club and non-rich-club organizations were strengthened.

Furthermore, the distribution of the three classified connections in the functional brain network was altered (Fig. 3C). In the wakefulness state, the intra-network rich-club connections were mainly located in the DMN, with some in the FPN, CON, and SMN. The inter-network rich-club connections were distributed in the connections between the DMN, FPN, CON, and SMN. However, the intra-network rich-club connections were transferred to the FPN and CN, and inter-network rich-club connections were mainly located in the connections of FPN, CON, and CN in the m-PIS state. Finally, the rich-club connections in the D-PIS state were intra-module and inter-module connections between the DMN and FPN. Meanwhile, we found the results of robustness for the costs of 12%, 15%, and 18%. These results suggest that the spatial distribution of rich-club connections was indeed affected by propofol. During propofol-induced unconsciousness, more rich-club connections were located in the intra-network connections of FPN and inter-network connections between FPN and other functional networks.

3.4. Rich-club analysis in natural sleep group

3.4.1. Distribution of rich-club regions during natural sleep

The same procedure of rich-club analysis was adopted for the sleep group as that of the PIS group. Importantly, for an unbiased comparison between the PIS and the sleep groups, the degree level of rich-club organization in the sleep group was altered to $k = 26$ to obtain similar numbers of rich-club regions (Fig. 4A). The rich-club organization for the different degree levels was shown in Supplementary Figure 8. For the sleep group, in both wakefulness and sleep states, the number and percentage of the rich-club nodes were the same: 17% and 10.63%, respectively (Fig. 4B). However, the distribution of rich-club nodes across the two states was different. Specifically, in the wakefulness state, most of the rich-club nodes were located in the DMN and others were uniformly distributed in the FPN (11.76%), SMN (5.88%), ON (11.76%), and CN (11.76%). In the sleep state, however, the rich-club nodes were mainly distributed in the DMN (29.41%), SMN (35.29%), and ON (17.65%), with others in the FPN (11.76%) and CON (5.88%). The details are shown in Fig. 4C. Furthermore, rich-club nodes during the wakefulness consisted of anterior and posterior cingulate cortex,

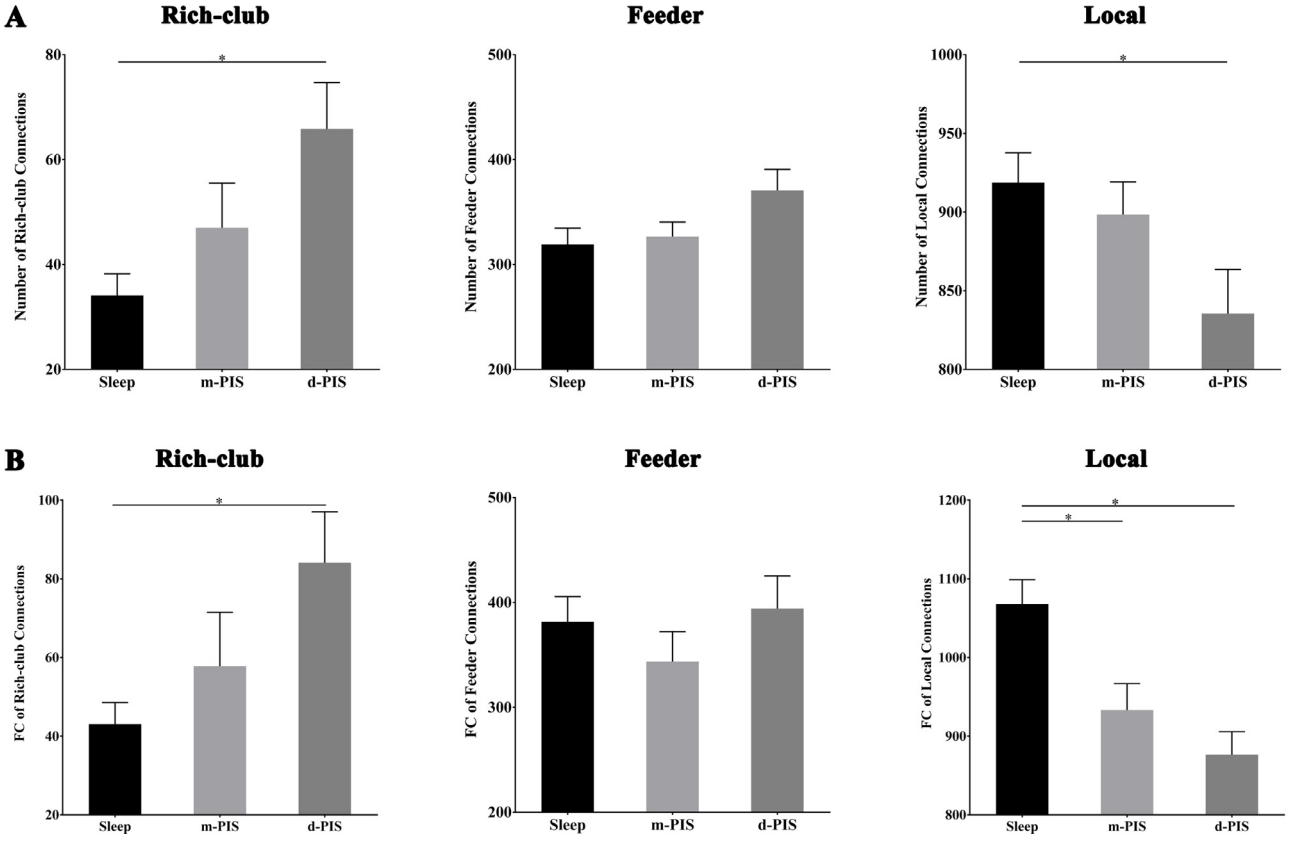

Fig. 6. The significant alteration in the number and strength of different categories of connections between PIS and sleep. (A) The significant alteration in the number of rich-club (left), feeder (middle) and local (right) connections between m-PIS and sleep. (B) The significant alteration in the strength of rich-club (left), feeder (middle) and local (right) connections between D-PIS and sleep. * represented the significant difference between the different states ($p < 0.05$). Error bar represented SEM.

angular gyrus, IPL, IPS, lateral cerebellum, PCC, precuneus, and occipital gyrus, while the rich-club nodes during the sleep state consisted of angular gyrus, dorsal and superior frontal cortex, middle insula, PCC, and a part of occipital and temporal lobes (Fig. 4D). These results suggest that the rich-club regions were transferred from the high-order cognitive systems network (DMN) and cerebellum system (CN) to the sensory systems (ON and SMN) during the process of unconsciousness induced by natural sleep. The details of rich-club distribution in the sleep group for the cost of 12%, 15%, and 18% are shown in Supplementary Figure 9 - 11. Along with the results of the rich-club organization in the PIS group, our findings suggest that the reorganization did occur in the loss of consciousness induced by both propofol and natural sleep. The transformation patterns of the rich-club regions, however, were slightly different.

3.5. The density of rich-club, feeder, and local connections

The number and strength of different categories of connections were not significantly different between wakefulness and sleep states ($p > 0.05$) (Fig. 5A and B). The details of different connection categories in the sleep group for the cost of 12%, 15%, and 18% are shown in Supplementary Figure 12–14. However, the distribution of rich-club connections was markedly altered in the sleep state compared with that in the wakefulness state. In the wakefulness state, rich-club and feeder connections were located in the intra-network connections of the DMN and inter-network connections between the DMN, FPN, and CN. In the sleep state, rich-club connections were located in the intra- and inter-networks of the DMN, FPN, SMN, CON, and ON. These results indicated that there was no global alteration in the different categories of connections in the sleep state. However, the spatial distributions of three categories of connections were different.

3.6. Connection alterations between propofol-induced sedation and natural sleep

To further investigate the alterations in different types of unconsciousness, the number and strength of different connection categories were compared between the sedation (m-PIS and d-PIS) and sleep states (Fig. 6A and B). Compared with the sleep state, the number and strength of rich-club connections were significantly increased in the d-PIS state (two-tail two-sample *t*-test, number: $T = 3.3887$, $p = 0.0041$; strength: $T = 3.0426$, $p = 0.0082$). Furthermore, the number and strength of local connections were significantly decreased (number: $T = -2.5037$, $p = 0.0243$; strength: $T = -4.4614$, $p = 0.0005$). There was no significant difference between the m-PIS and sleep states, except for the strength of local connections ($T = -2.9496$, $p = 0.0099$). Combined with the above results, these results indicate that the pattern of rich-club reorganization in the functional brain network could distinguish propofol-induced unconsciousness from sleep-induced unconsciousness.

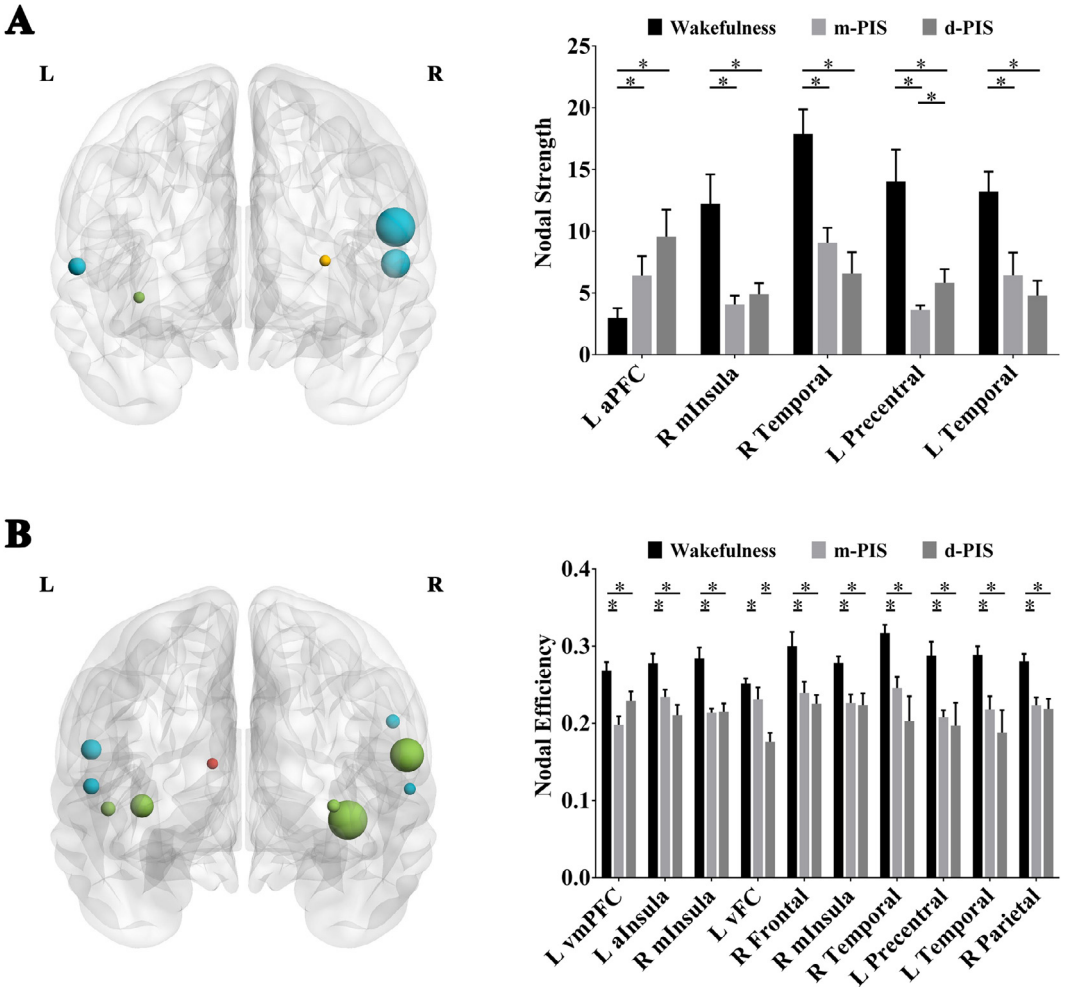

Fig. 7. The significant alteration of the topological properties in the PIS group. (A) The significant alteration of nodal strength. (B) The significant alteration of nodal efficiency. Left: The distribution of the significantly altered brain region. The larger size of the ball represented the smaller p-value. The different colors represented different brain functional networks. As was shown in Fig. 1. Right: The detailed significant alteration of brain regions between the different states. * represented the significant difference between the different states ($p < 0.05$, FDR correction for 160 nodes). Error bar represented SEM.(For interpretation of the references to colour in this figure legend, the reader is referred to the web version of this article.)

3.7. The analysis of local topological properties

3.7.1. Decreased nodal strength and efficiency in pis states

We further investigated the local alterations of rich-club and non-rich-club regions from consciousness to unconsciousness induced by propofol. In graph theory and network analysis, the basic and common topological properties of weighted networks are nodal strength and nodal efficiency (Rubinov and Sporns, 2010). Previous studies have indicated that rich-clubs play a central role in the overall brain network and have a strong positive impact on the global efficiency of the network (Daianu et al., 2015; Harriger et al., 2012; Li et al., 2017; van den Heuvel and Sporns, 2011). Therefore, we identified the brain regions showing significant inter-group differences in the local topological properties, including nodal strength and nodal efficiency. Compared with the wakefulness state, during m-PIS and D-PIS, nodal strength was significantly decreased in the right middle insula, bilateral temporal gyrus, and left precentral gyrus and significantly increased in the left anterior prefrontal cortex. When compared with the m-PIS state, the nodal strength of the left precentral gyrus was significantly high in the D-PIS state. The details are shown in Fig. 7A. When compared with the wakefulness state, nodal efficiency was significantly high in the left ventral medial PFC (vmPFC), left anterior insula (aInsula), right middle insula, right frontal gyrus, left precentral gyrus, right parietal gyrus and bilateral temporal gyrus during the PIS state. Moreover, the nodal efficiency of the left ventral frontal cortex (vFC) was markedly decreased in the D-PIS, compared with that in the wakefulness and m-PIS states (Fig. 7B). All p values of nodal topological properties in significantly altered regions were less than 0.05 after the FDR correction.

3.8. Alteration of nodal strength and efficiency in natural sleep state

In this study, we also studied alterations in the local topological properties of the functional brain networks during the sleep states. When compared with the wakefulness state, nodal strength was significantly decreased in the right pre-supplementary motor area (preSMA) and right precuneus during the sleep state; in contrast, it was significantly increased in the left parietal and temporal gyrus. Nodal efficiency was also significantly decreased in the right preSMA and precuneus and was markedly increased in the left temporal gyrus (Fig. 8A and B).

3.9. Decreased efficiency in the pis states compared with natural sleep

When compared with the sleep state, nodal efficiency was significantly decreased in the right anterior and middle insula, right dorsal frontal cortex (dFC), left precentral gyrus, left temporal gyrus, and right parietal gyrus during the m-PIS state. Nodal efficiency was also significantly decreased in the right ventral lateral prefrontal cortex (vlPFC), right dFC, bilateral vFC, left precentral, left middle insula (mInsula), right PCC, left temporal and left cerebellum (Fig. 9A and B).

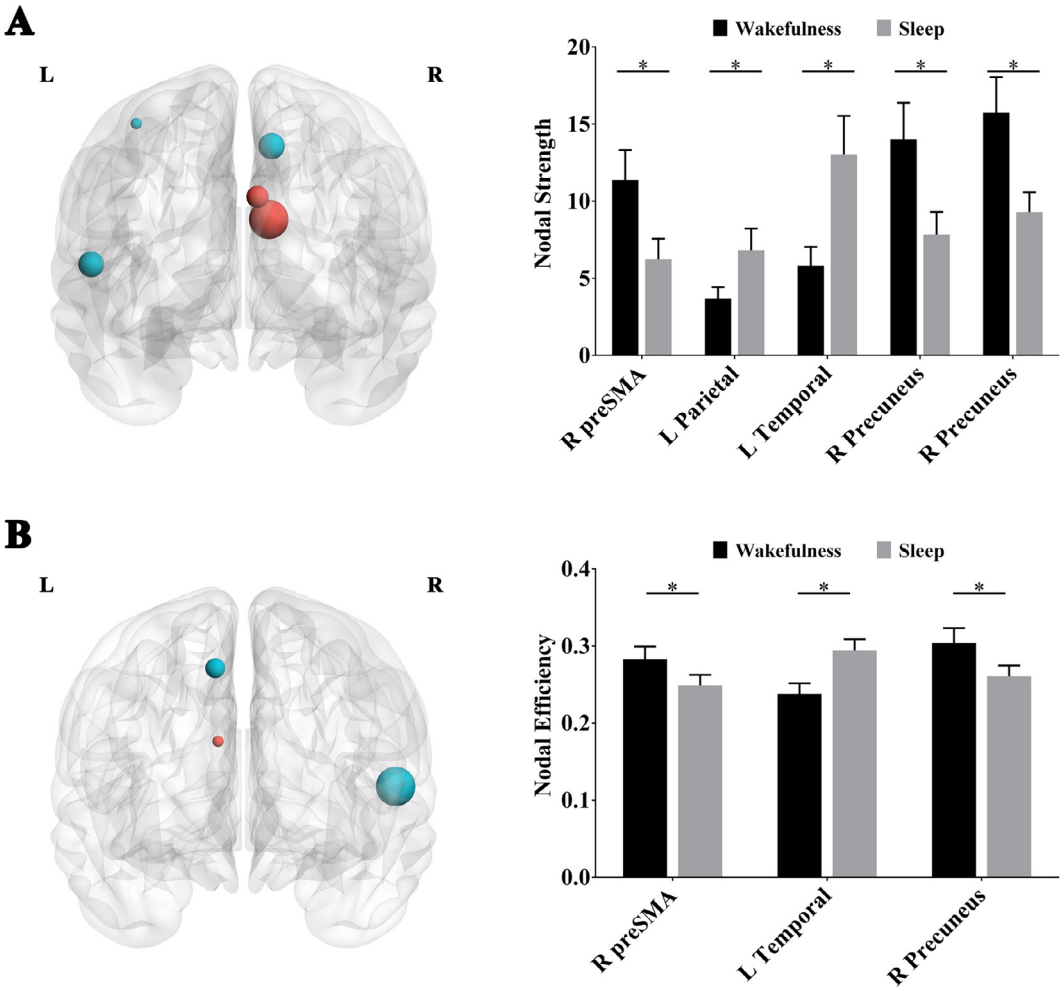

Fig. 8. The significant alteration of the topological properties in the sleep group. (A) The significant alteration of nodal strength. (B) The significant alteration of nodal efficiency. Left: The distribution of the significantly altered brain region. The larger size of the ball represented the smaller p-value. The different colors represented different brain functional networks. As was shown in Fig. 1. Right: The detailed significant alteration of brain regions between wakefulness and sleep. * represented the significant difference between the different states ($p < 0.05$, FDR correction for 160 nodes). Error bar represented SEM.(For interpretation of the references to colour in this figure legend, the reader is referred to the web version of this article.)

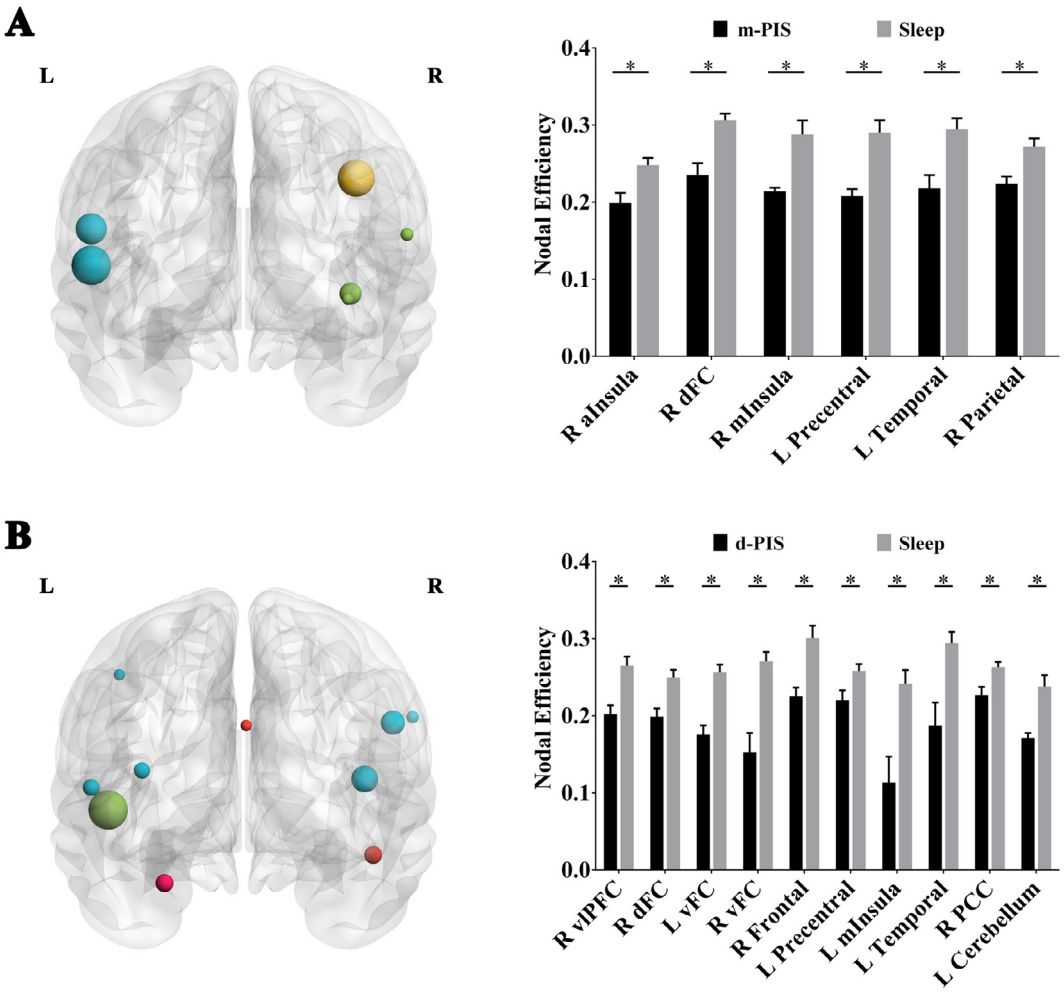

Fig. 9. The significant alteration of the topological properties between PIS and sleep. (A) The significant alteration of nodal efficiency between m-PIS and sleep. (B) The significant alteration of nodal efficiency between D-PIS and sleep. Left: The distribution of the significantly altered brain region. The larger size of the ball represented the smaller p-value. The different colors represented different brain functional networks. As was shown in Fig. 1. Right: The detailed significant alteration of brain regions between wakefulness and sleep. * represented the significant difference between the different states ($p < 0.05$, FDR correction for 160 nodes). Error bar represented SEM.

4. Discussion

Rich-club organization exhibits a complex network relationship across many different brain regions and carries out the most efficient information transfer throughout the brain (Ball et al., 2014). Understanding the changes in the rich-club organization of the functional brain network during propofol-induced unconsciousness together with natural sleep-based unawareness will bring new insights into the understanding of neurobiological mechanisms of intravenous GA. In this study, the rich-club organizations in functional brain networks were constructed by rs-fMRI. These constructions were then compared between the two behaviorally similar responsive states: during progressively induced waking-mild-deep sedation by propofol and natural sleep. This led to some interesting discoveries that could explain the clinical and experimental findings reported in previous GA mechanism studies.

4.1. Rich-club reorganization during propofol-induced sedation

Prior studies have highlighted that rich-clubs of networks play a central role in the overall network structure (van den Heuvel and Sporns, 2011; Xu et al., 2010). A recent study examined the damage inflicted by attacks on rich-club nodes and found that attacks that specifically targeted rich-club connections impaired the global efficiency approximately three times more than the attacks that were randomly distributed (Harriger et al., 2012; van den Heuvel and Sporns, 2011). These results have suggested that the overall communications in the brain are dominantly controlled by the rich-club organization. Meanwhile, the central role of rich-club regions in long-distance brain communications is in agreement with the recent functional connectivity studies, which have shown that the functional hubs play an important role in optimizing the global brain communication efficiency for healthy cognitive brain functioning (Collin et al., 2014; Reus and van den Heuvel, 2013; van den Heuvel and Sporns, 2011). In the functional brain communication area, our study is the first to propose that the rich-club organization is differentially modified by the alteration of consciousness gradually induced by propofol. It is important to note that the rich-club connections were not disrupted but reorganized during the gradual process of losing behavioral responsiveness. The above results indicate that the mechanism of propofol-induced unconsciousness is closely related to the redistribution of brain hubs in the functional networks.

4.2. The transformation pattern of rich-club regions during propofol-induced sedation

In particular, our study has shown that the rich-club regions are transferred between high-level cognitive networks (DMN and FPN),

sensory and motor networks (SMN and ON), and cerebellum network (CN) during the whole process of unconsciousness induced by propofol. These are in line with the previous finding (Boveroux et al., 2010) that the correlation between decreased connectivity and propofol-induced decrease in consciousness is a general rule in most areas of default network and executive control networks. On the contrary, no relationship between connectivity and consciousness could be identified in early visual and auditory cortices. Moreover, under the influence of propofol, a large number of connections were switched over to rich-club connections from local connections.

Our findings are also in agreement with previous studies that have demonstrated that the topological parameters of brain regions are disrupted within the DMN and FPN in the impaired consciousness from rs-fMRI and EEG perspectives, respectively (Crone et al., 2015, 2014; Long et al., 2016; Uehara et al., 2014). A recent study also confirms the previous finding implying the involvement of FPN and DMN, highlighting specific interactions in the network-level topology that may play a key role in mediating consciousness (Lee et al., 2013). The FPN is thought to be involved in control and attention (Corbetta and Shulman, 2002; Wang et al., 2016) and plays a central role in the cognitive control and adaptive implementation of task demands (Cole et al., 2013). Moreover, previous studies also revealed a critical role for FPN in switching between the central-executive and the default-mode network. Also, the FPN might be responsible for controlling the coordination and planning of the complex motor functions (He et al., 2013; Hsu et al., 2017). The EEG-based study on GA indicated that the frontal-parietal connectivity was disrupted during PIS (Kim et al., 2017). Some studies have shown that the response of the auditory cortex to sound stimuli was reduced in different degrees of sedation with propofol, but it was still present (Dueck et al., 2005; Liu et al., 2015). Auditory cortex response to sound stimuli was not completely blocked when alertness disappeared with a large dose of propofol, but the specific responses to different sounds and vocabulary stimuli were lost (Plourde et al., 2006). The level of alertness depends on the effective change, exchanges, and integration of the information between the cortexes (Tononi, 2004). Here, we argue that the transformation and redistribution of hubs from high-level cognitive networks and sensory to motor networks might be the important characterization of unconsciousness induced by propofol.

The number of rich-club regions in the cerebellum network was also significantly altered during the PIS. The cerebellum is traditionally thought to be related to motor functions. It receives inputs from the sensory system of the spinal cord or cortical and subcortical regions and integrates these inputs to fine-tune the motor activity (Thach, 1998). The cerebellum is involved in various functions, including motor speech control, oculomotor functions, grip forces, voluntary limb movement, and classical conditioning (Manto et al., 2012). The cerebellum is also involved in neural correlations of auditory consciousness, detailed memory retrieval, and trait anxiety (Eriksson, 2017; Poerio et al., 2017; Yin et al., 2016). An animal study has also proved the importance of the cerebellum in maintaining consciousness (Schroeder et al., 2016). The cerebellar-cerebral connectivity modulation may be an indication of the ameliorating level of consciousness (Naro et al., 2016). A recent study showed that the activation of the cerebellum was decreased during propofol-induced sedation and the early recovery period (Shinohe et al., 2016). In essence, the cerebellum may play an important role in maintaining wakefulness and thus can serve as a major target for general anesthetics.

4.3. Strengthened communication of rich-club organization during propofol-induced sedation

A previously reported study has found that the connectivity among a fairly small number of rich-club regions dominated the aggregation throughout the whole brain network, revealing that the rich-club connectivity is leveraged throughout the network (Xu et al., 2010). Modulating the connectivity pattern in a very small rich-club is sufficient to produce a network with desired assortativity or transitivity. These results indicated that rich-club connections play an important role in brain network communication (Xu et al., 2010). In our study, the number and strength of rich-club connections were modulated by propofol. In particular, compared with wakefulness, the number and strength of the rich-club connections were significantly increased, while the number and strength of the local connections were significantly decreased during the D-PIS. Additionally, the number and strength of the rich-club, feeder, and local connections were not significantly different between the m-PIS and wakefulness states. Our findings indicate that more rich-club connections are needed to promote the communication of the whole brain during propofol-induced unconsciousness. Additionally, it is worth mentioning that the definition of “intrinsic connectivity networks” leads to a step towards comprehending the possible action targets of propofol anesthesia (Damoiseaux et al., 2006; Seeley et al., 2007; Song and Yu, 2015). These networks consist of the DMN, the executive control network (ECN), the visual and auditory networks (Boly et al., 2008; Mason et al., 2007). They are higher-order information processing networks to support the emergence of mental content and inner self (Bonhomme et al., 2011). Our study has already revealed that the rich-club connectivity distribution was gradually converting at the period of propofol-induced unconsciousness. Particularly, intra-network rich-club connections of high-order cognitive networks (DMN and FPN) were significantly enhanced, including the inter-network connections between high-order networks and sensory and motion networks. On the contrary, the intra-network rich-club connections of the sensory and motor networks (SMN) were significantly attenuated. These findings were consistent with the previous studies, which indicated that the propofol-induced disconnections might occur within the core regions of the low-order RSNs (Boveroux et al., 2010; Guldenmund et al., 2016), such as the intra-network connectivity between the auditory and visual networks (Boveroux et al., 2010). Our results also suggest that the high-order processing networks for verbal processing and memory become closely connected with the sensory network during deep propofol sedation. In brief, communication between the sensory cortices and high-order fronto-parietal cortices was enhanced in propofol-induced unconsciousness, but the intra-network communication between the low-order networks was disturbed. All these results suggest that studying the distribution of rich-club connections provides an insight into the mechanism of functional interactions among the brain regions under the influence of propofol.

4.4. Functional network differences between physiological and pharmacological unconsciousness

Sedation is usually thought to be an analog of sleep because most of the recalls from the subjects who have received sedation are depicted as sleeping, however, they are two separate unconsciousness states (Brown et al., 2010; Franks and Zecharia, 2011; Vacas et al., 2013). As a whole, the rich-club transfer pattern under the propofol action from high-level cognitive networks to sensory and motor networks was similar to that in the natural sleep in our study. However, the distribution of rich-club regions and connections between the propofol-induced unconsciousness and natural sleep were very different. Moreover, when compared with the natural sleep, the strength and number of rich-club connections were significantly increased, and that of the local connections were significantly decreased during the D-PIS. A reduction in network efficiency was observed in both local and global brain networks during the anesthetic-induced unconsciousness (Hashmi et al., 2017; Mashour and Hudetz, 2018; Monti et al., 2013). These results indicate that the functional brain networks have better assortativity or transitivity but less efficiency during the anesthetic-induced unconsciousness than natural sleep.

We have also found some similar features between the

unconsciousness induced by propofol and natural sleep. The rich-club regions located in the bilateral angular gyrus and posterior occipital gyrus were the same in both cases. Previous studies have reported consistent findings that both propofol-induced unconsciousness and slow-wave sleep were associated with a reduction of blood flow in the angular gyri (Fiset et al., 1999; Gagnon et al., 2012; Song and Yu, 2015). However, the rich-club regions located in the left ACC and bilateral IPL and IPS only appeared in unconsciousness induced by propofol, while rich-club regions located in the right superior and dorsal frontal cortex, right PCC, left posterior parietal gyrus, and the bilateral temporal gyrus appeared only during natural sleep. In summary, nodal efficiency in the frontal gyrus, precentral gyrus, middle insula, PCC, and cerebellum can be used as a measure for differentiating between anesthetic- and sleep-induced unconsciousness.

4.5. Limitations

The current study potentially offers a novel perspective in understanding the neurological mechanism of propofol-induced sedation on a systematic level, but the key limitations cannot be ignored. Firstly, the size of participants in our study was relatively small (17 healthy volunteers, including 8 participants in the PIS and 9 participants in the sleep group), which may have biased the findings of the study. Some important factors were also not considered, such as individual variations. The larger sample size is required in future research to support the findings of the present study. Secondly, the acquisition time of data in the sleep state was not the same as the physiological timetable of individuals due to the limitations of the conditions. A more rigorous, through study and a better scientific experimental design is needed to cope up with the effects of other factors and to verify the current findings in the future.

5. Conclusion

Loss of consciousness induced by propofol produced widespread changes in the rich-club organization in the human brain and targeted the rich-club reorganization from the high-order cognitive networks (DMN and FPN) to the primary sensory cortices (SMN and ON) and cerebellum network. The overall information commutation of the functional brain networks was strengthened during the propofol-induced alteration of consciousness. Physiological natural sleep also showed a similar rich-club reorganization pattern. The rich-club regions were switched from the high-order cognitive networks (DMN) to the sensorimotor network (SMN, including part of the frontal and temporal gyrus) (Bullmore and Bassett, 2011). These findings suggest that the rich-club reorganization of the brain networks might be the common underlying neurological mechanism of physiological and pharmacological unconsciousness. Moreover, compared with the natural sleep, the nodal efficiency of hubs, including the insula, posterior cingulate cortex, frontal gyrus, and cerebellum, were significantly decreased during propofol-induced unconsciousness. This suggests that the local topological properties may be used as a measure to distinguish between the pharmacologic and physiological unconsciousness. In the future, the hub reorganization pattern should be studied in other drug-induced unconsciousness states to determine the neurological mechanism of GA and its connection with slow-wave sleep.

6. Clinical trial number and registry URL

Registry: Chinese Clinical Trial Registry.
Clinical trial registration number: ChiCTR-IOC-15007454.
Principal investigator's name: Yun Li.
Date of registration: 2015–11–25.

Declaration of Competing Interest

The authors declare no competing interests.

Acknowledgments

This work was supported by the National Natural Science Foundation of China (61976209, 81701785), CAS International Collaboration Key Project, and the Strategic Priority Research Program of CAS (XDB32040200).

Supplementary materials

Supplementary material associated with this article can be found, in the online version, at doi:10.1016/j.nicl.2020.102188.

References

Absalom, A.R., Mani, V., Smet, T., Struys, M.M.R.F., 2009. Pharmacokinetic models for propofol-defining and illuminating the devil in the detail. Br. J. Anaesth. 103 (1), 26–37. https://doi.org/10.1093/bja/aep143.

Adapa, R.M., Axell, R.G., Mangat, J.S., Carpenter, T.A., Absalom, A.R., 2012. Safety and performance of TCI pumps in a magnetic resonance imaging environment. Anaesthesia 67 (1), 33–39. https://doi.org/10.1111/j.1365-2044.2011.06917.x.

Albert, Jeong Barabasi, 2000. Error and attack tolerance of complex networks. Nature 406 (6794), 378–382. https://doi.org/10.1038/35019019.

Alkire, M.T., Hudetz, A.G., Tononi, G., 2008. Consciousness and anesthesia. Science 322 (5903), 876–880. https://doi.org/10.1126/science.1149213. (New York, N.Y.).

Alkire, M.T., Miller, J., 2005. General anesthesia and the neural correlates of consciousness. Prog. Brain Res. 150, 229–244. https://doi.org/10.1016/S0079-6123(05)50017-7.

Angel, A., 1993. Central neuronal pathways and the process of anaesthesia. Br. J. Anaesth. 71 (1), 148–163. https://doi.org/10.1093/bja/71.1.148.

Baars, B.J., Ramsøy, T.Z., Laureys, S., 2003. Brain, conscious experience and the observing self. Trends Neurosci. 26 (12), 671–675. https://doi.org/10.1016/j.tins.2003.09.015.

Ball, G., Aljabar, P., Zebari, S., Tusor, N., Arichi, T., Merchant, N., Robinson, E.C., Ogundipe, E., Rueckert, D., Edwards, A.D., Counsell, S.J., 2014. Rich-club organization of the newborn human brain. In: Proceedings of the National Academy of Sciences of the United States of America. 111. pp. 7456–7461. https://doi.org/10.1073/pnas.1324118111.

Barabasi, Albert, 1999. Emergence of scaling in random networks. Science 286 (5439), 509–512 (New York, N.Y.).

Boly, M., Phillips, C., Balteau, E., Schnakers, C., Degueldre, C., Moonen, G., Luxen, A., Peigneux, P., Faymonville, M.-E., Maquet, P., Laureys, S., 2008. Consciousness and cerebral baseline activity fluctuations. Hum. Brain Mapp. 29 (7), 868–874. https://doi.org/10.1002/hbm.20602.

Bonhomme, V., Boveroux, P., Hans, P., Brichant, J.F., Vanhaudenhuyse, A., Boly, M., Laureys, S., 2011. Influence of anesthesia on cerebral blood flow, cerebral metabolic rate, and brain functional connectivity. Curr. Opin. Anaesthesiol. 24 (5), 474–479. https://doi.org/10.1097/ACO.0b013e32834a12a1.

Bonhomme, V., Vanhaudenhuyse, A., Demertzi, A., Bruno, M.-A., Jaquet, O., Bahri, M.A., Plenevaux, A., Boly, M., Boveroux, P., Soddu, A., Brichant, J.F., Maquet, P., Laureys, S., 2016. Resting-state network-specific breakdown of functional connectivity during ketamine alteration of consciousness in volunteers. Anesthesiology 125 (5), 873–888. https://doi.org/10.1097/ALN.0000000000001275.

Boveroux, P., Vanhaudenhuyse, A., Bruno, M.-A., Noirhomme, Q., Lauwick, S., Luxen, A., Degueldre, C., Plenevaux, A., Schnakers, C., Phillips, C., Brichant, J.-F., Bonhomme, V., Maquet, P., Greicius, M.D., Laureys, S., Boly, M., 2010. Breakdown of within- and between-network resting state functional magnetic resonance imaging connectivity during propofol-induced loss of consciousness. Anesthesiology 113 (5), 1038–1053. https://doi.org/10.1097/ALN.0b013e3181f697f5.

Boyacioglu, R., Beckmann, C.F., Barth, M., 2013. An investigation of rsn frequency spectra using ultra-fast generalized inverse imaging. Front. Hum. Neurosci. 7. https://doi.org/10.3389/fnhum.2013.00156.

Brown, E.N., Lydic, R., Schiff, N.D., 2010. General anesthesia, sleep, and coma. New Engl. J. Med. 363 (27), 2638–2650. https://doi.org/10.1056/NEJMra0808281.

Bullmore, E.T., Bassett, D.S., 2011. Brain graphs: graphical models of the human brain connectome. Annu. Rev. Clin. Psychol. 7, 113–140. https://doi.org/10.1146/annurev-clinpsy-040510-143934.

Campagna, J.A., Miller, K.W., Forman, S.A., 2003. Mechanisms of actions of inhaled anesthetics. New Engl. J. Med. 348 (21), 2110–2124. https://doi.org/10.1056/NEJMra021261.

Cao, M., Wang, J.-H., Dai, Z.-J., Cao, X.-Y., Jiang, L.-L., Fan, F.-M., Song, X.-W., Xia, M.-R., Shu, N., Dong, Q., Milham, M.P., Castellanos, F.X., Zuo, X.-N., He, Y., 2014. Topological organization of the human brain functional connectome across the lifespan. Dev. Cogn. Neurosci. 7, 76–93. https://doi.org/10.1016/j.dcn.2013.11.004.

Chai, X.J., Castañón, A.N., Ongür, D., Whitfield-Gabrieli, S., 2012. Anticorrelations in resting state networks without global signal regression. Neuroimage 59 (2), 1420–1428. https://doi.org/10.1016/j.neuroimage.2011.08.048.

Chen, J.E., Glover, G.H., 2015. BOLD fractional contribution to resting-state functional connectivity above 0.1 Hz. Neuroimage 107, 207–218. https://doi.org/10.1016/j.neuroimage.2014.12.012.
Choe, A.S., Nebel, M.B., Barber, A.D., Cohen, J.R., Xu, Y., Pekar, J.J., Caffo, B., Lindquist, M.A., 2017. Comparing test-retest reliability of dynamic functional connectivity methods. Neuroimage 158, 155–175. https://doi.org/10.1016/j.neuroimage.2017.07.005.
Cole, M.W., Reynolds, J.R., Power, J.D., Repovs, G., Anticevic, A., Braver, T.S., 2013. Multi-task connectivity reveals flexible hubs for adaptive task control. Nat. Neurosci. 16 (9), 1348–1355. https://doi.org/10.1038/nn.3470.
Colizza, v, Flammini, A., Serrano, M.A., Vespignani, A., 2006. Detecting rich-club ordering in complex networks. Nature Phys. 2 (2), 110–115. https://doi.org/10.1038/nphys209.
Collin, G., Sporns, O., Mandl, R.C.W., van den Heuvel, M.P., 2014. Structural and functional aspects relating to cost and benefit of rich club organization in the human cerebral cortex. Cerebral Cortex 24 (9), 2258–2267. https://doi.org/10.1093/cercor/bht064. (New York, N.Y.: 1991).
Collins, J.G., Kendig, J.J., Mason, P., 1995. Anesthetic actions within the spinal cord: contributions to the state of general anesthesia. Trends Neurosci. 18 (12), 549–553.
Corbetta, M., Shulman, G.L., 2002. Control of goal-directed and stimulus-driven attention in the brain. Nat. Rev. Neurosci. 3 (3), 201–215. https://doi.org/10.1038/nrn755.
Cordes, D., Haughton, V.M., Arfanakis, K., Carew, J.D., Turski, P.A., Moritz, C.H., Quigley, M.A., Meyerand, M.E., 2001. Frequencies contributing to functional connectivity in the cerebral cortex in "resting-state" data. AJNR Am. J. Neuroradiol. 22 (7), 1326–1333.
Craig, M.M., Manktelow, A.E., Sahakian, B.J., Menon, D.K., Stamatakis, E.A., 2018. Spectral diversity in default mode network connectivity reflects behavioral state. J. Cogn. Neurosci. 30 (4), 526–539. https://doi.org/10.1162/jocn_a_01213.
Crone, J.S., Schurz, M., Höller, Y., Bergmann, J., Monti, M., Schmid, E., Trinka, E., Kronbichler, M., 2015. Impaired consciousness is linked to changes in effective connectivity of the posterior cingulate cortex within the default mode network. Neuroimage 110, 101–109. https://doi.org/10.1016/j.neuroimage.2015.01.037.
Crone, J.S., Soddu, A., Höller, Y., Vanhaudenhuyse, A., Schurz, M., Bergmann, J., Schmid, E., Trinka, E., Laureys, S., Kronbichler, M., 2014. Altered network properties of the fronto-parietal network and the thalamus in impaired consciousness. Neuroimage Clin. 4, 240–248. https://doi.org/10.1016/j.nicl.2013.12.005.
Csigi, M., Kőrösi, A., Bíró, J., Heszberger, Z., Malkov, Y., Gulyás, A., 2017. Geometric explanation of the rich-club phenomenon in complex networks. Sci. Rep. 7. https://doi.org/10.1038/s41598-017-01824-y.
Daianu, M., Jahanshad, N., Nir, T.M., Jack, C.R., Weiner, M.W., Bernstein, M.A., Thompson, P.M., 2015. Rich club analysis in the alzheimer's disease connectome reveals a relatively undisturbed structural core network. Hum. Brain Mapp. 36 (8), 3087–3103. https://doi.org/10.1002/hbm.22830.
Damoiseaux, J.S., Rombouts, S.A.R.B., Barkhof, F., Scheltens, P., Stam, C.J., Smith, S.M., Beckmann, C.F., 2006. Consistent resting-state networks across healthy subjects. Proc. Natl. Acad. Sci. U.S.A. 103 (37), 13848–13853. https://doi.org/10.1073/pnas.0601417103.
Dosenbach, N.U.F., Nardos, B., Cohen, A.L., Fair, D.A., Power, J.D., Church, J.A., Nelson, S.M., Wig, G.S., Vogel, A.C., Lessov-Schlaggar, C.N., Barnes, K.A., Dubis, J.W., Feczko, E., Coalson, R.S., Pruett, J.R., Barch, D.M., Petersen, S.E., Schlaggar, B.L., 2010. Prediction of individual brain maturity using fMRI. Science 329 (5997), 1358–1361. https://doi.org/10.1126/science.1194144. (New York, N.Y.).
Dueck, M.H., Petzke, F., Gerbershagen, H.J., Paul, M., Hesselmann, V., Girnus, R., Krug, B., Sorger, B., Goebel, R., Lehrke, R., Sturm, V., Boerner, U., 2005. Propofol attenuates responses of the auditory cortex to acoustic stimulation in a dose-dependent manner: a FMRI study. Acta Anaesthesiol. Scand. 49 (6), 784–791. https://doi.org/10.1111/j.1399-6576.2005.00703.x.
Eikermann, M., Vetrivelan, R., Grosse-Sundrup, M., Henry, M.E., Hoffmann, U., Yokota, S., Saper, C.B., Chamberlin, N.L., 2011. The ventrolateral preoptic nucleus is not required for deep isoflurane general anesthesia. Brain Res. 1426, 30–37. https://doi.org/10.1016/j.brainres.2011.10.018.
Eriksson, J., 2017. Activity in part of the neural correlates of consciousness reflects integration. Conscious. Cogn. 55, 26–34. https://doi.org/10.1016/j.concog.2017.07.007.
Evers, A.S., Crowder, C.M., 2006. Cellular and molecular mechanisms of anesthesia. Clin. Anesth. 5, 111–132.
Feindel, W., 1991. The montreal neurological institute. J. Neurosurg. 75 (5), 821–822. https://doi.org/10.3171/jns.1991.75.5.0821.
Fiset, P., Paus, T., Daloze, T., Plourde, G., Meuret, P., Bonhomme, V., Hajj-Ali, N., Backman, S.B., Evans, A.C., 1999. Brain mechanisms of propofol-induced loss of consciousness in humans: a positron emission tomographic study. J. Neurosci. 19 (13), 5506–5513.
Fox, M.D., Zhang, D., Snyder, A.Z., Raichle, M.E., 2009. The global signal and observed anticorrelated resting state brain networks. J. Neurophysiol. 101 (6), 3270–3283. https://doi.org/10.1152/jn.90777.2008.
Franks, N.P., 2008. General anaesthesia: from molecular targets to neuronal pathways of sleep and arousal. Nat. Rev. Neurosci. 9 (5), 370–386. https://doi.org/10.1038/nrn2372.
Franks, N.P., Zecharia, A.Y., 2011. Sleep and general anesthesia. Can. J. Anaesth. 58 (2), 139–148. https://doi.org/10.1007/s12630-010-9420-3.
Friston, K.J., Williams, S., Howard, R., Frackowiak, R.S., Turner, R., 1996. Movement-related effects in fMRI time-series. Magn. Reson. Med. 35 (3), 346–355. https://doi.org/10.1002/mrm.1910350312.
Gagnon, J.-F., Bertrand, J.-A., Génier Marchand, D., 2012. Cognition in rapid eye movement sleep behavior disorder. Front. Neurol. 3. https://doi.org/10.3389/fneur.2012.00082.
Gohel, S.R., Biswal, B.B., 2015. Functional integration between brain regions at rest occurs in multiple-frequency bands. Brain Connect. 5 (1), 23–34. https://doi.org/10.1089/brain.2013.0210.
Gotts, S.J., Saad, Z.S., Jo, H.J., Wallace, G.L., Cox, R.W., Martin, A., 2013. The perils of global signal regression for group comparisons: a case study of autism spectrum disorders. Front. Hum. Neurosci. 7, 356. https://doi.org/10.3389/fnhum.2013.00356.
Greicius, M.D., Kiviniemi, V., Tervonen, O., Vainionpää, V., Alahuhta, S., Reiss, A.L., Menon, V., 2008. Persistent default-mode network connectivity during light sedation. Hum. Brain Mapp. 29 (7), 839–847. https://doi.org/10.1002/hbm.20537.
Guldenmund, P., Demertzi, A., Boveroux, P., Boly, M., Vanhaudenhuyse, A., Bruno, M.-A., Gosseries, O., Noirhomme, Q., Brichant, J.-F., Bonhomme, V., Laureys, S., Soddu, A., 2013. Thalamus, brainstem and salience network connectivity changes during propofol-induced sedation and unconsciousness. Brain Connect. 3 (3), 273–285. https://doi.org/10.1089/brain.2012.0117.
Guldenmund, P., Gantner, I.S., Baquero, K., Das, T., Demertzi, A., Boveroux, P., Bonhomme, V., Vanhaudenhuyse, A., Bruno, M.-A., Gosseries, O., Noirhomme, Q., Kirsch, M., Boly, M., Owen, A.M., Laureys, S., Gómez, F., Soddu, A., 2016. Propofol-Induced frontal cortex disconnection: a study of resting-state networks, total brain connectivity, and mean bold signal oscillation frequencies. Brain Connect. 6 (3), 225–237. https://doi.org/10.1089/brain.2015.0369.
Guldenmund, P., Vanhaudenhuyse, A., Sanders, R.D., Sleigh, J., Bruno, M.A., Demertzi, A., Bahri, M.A., Jaquet, O., Sanfilippo, J., Baquero, K., Boly, M., Brichant, J.F., Laureys, S., Bonhomme, V., 2017. Brain functional connectivity differentiates dexmedetomidine from propofol and natural sleep. Br. J. Anaesth. 119 (4), 674–684. https://doi.org/10.1093/bja/aex257.
Harriger, L., van den Heuvel, M.P., Sporns, O., 2012. Rich club organization of macaque cerebral cortex and its role in network communication. PLoS ONE 7 (9), e46497. https://doi.org/10.1371/journal.pone.0046497.
Hashmi, J.A., Loggia, M.L., Khan, S., Gao, L., Kim, J., Napadow, V., Brown, E.N., Akeju, O., 2017. Dexmedetomidine disrupts the local and global efficiencies of large-scale brain networks. Anesthesiology 126 (3), 419–430. https://doi.org/10.1097/ALN.0000000000001509.
He, X., Qin, W., Liu, Y., Zhang, X., Duan, Y., Song, J., Li, K., Jiang, T., Yu, C., 2013. Age-related decrease in functional connectivity of the right fronto-insular cortex with the central executive and default-mode networks in adults from young to middle age. Neurosci. Lett. 544, 74–79. https://doi.org/10.1016/j.neulet.2013.03.044.
Heine, L., Soddu, A., Gómez, F., Vanhaudenhuyse, A., Tshibanda, L., Thonnard, M., Charland-Verville, V., Kirsch, M., Laureys, S., Demertzi, A., 2012. Resting state networks and consciousness: alterations of multiple resting state network connectivity in physiological, pharmacological, and pathological consciousness states. Front. Psychol. 3, 295. https://doi.org/10.3389/fpsyg.2012.00295.
Holme, P., Kim, B.J., Yoon, C.N., Han, S.K., 2002. Attack vulnerability of complex networks. Phys. Rev. E Stat. Nonlin. Soft Matter Phys. 65 (5 Pt 2), 56109. https://doi.org/10.1103/PhysRevE.65.056109.
Hsu, C.L., Best, J.R., Wang, S., Voss, M.W., Hsiung, R.G.Y., Munkacsy, M., Cheung, W., Handy, T.C., Liu-Ambrose, T., 2017. The impact of aerobic exercise on fronto-parietal network connectivity and its relation to mobility: an exploratory analysis of a 6-month randomized controlled trial. Front. Hum. Neurosci. 11, 344. https://doi.org/10.3389/fnhum.2017.00344.
Huang, Z., Liu, X., Mashour, G.A., Hudetz, A.G., 2018a. Timescales of intrinsic bold signal dynamics and functional connectivity in pharmacologic and neuropathologic states of unconsciousness. J. Neurosci. 38 (9), 2304–2317. https://doi.org/10.1523/JNEUROSCI.2545-17.2018.
Huang, Z., Zhang, J., Wu, J., Liu, X., Xu, J., Zhang, J., Qin, P., Dai, R., Yang, Z., Mao, Y., Hudetz, A.G., Northoff, G., 2018b. Disrupted neural variability during propofol-induced sedation and unconsciousness. Hum. Brain Mapp. 39 (11), 4533–4544. https://doi.org/10.1002/hbm.24304.
Hudetz, A.G., Mashour, G.A., 2016. Disconnecting consciousness: is there a common anesthetic end point? Anesth. Analg. 123 (5), 1228–1240. https://doi.org/10.1213/ANE.0000000000001353.
Jordan, D., Ilg, R., Riedl, V., Schorer, A., Grimberg, S., Neufang, S., Omerovic, A., Berger, S., Untergehrer, G., Preibisch, C., Schulz, E., Schuster, T., Schröter, M., Spoormaker, V., Zimmer, C., Hemmer, B., Wohlschläger, A., Kochs, E.F., Schneider, G., 2013. Simultaneous electroencephalographic and functional magnetic resonance imaging indicate impaired cortical top-down processing in association with anesthetic-induced unconsciousness. Anesthesiology 119 (5), 1031–1042. https://doi.org/10.1097/ALN.0b013e3182a7ca92.
Keller, C.J., Bickel, S., Honey, C.J., Groppe, D.M., Entz, L., Craddock, R.C., Lado, F.A., Kelly, C., Milham, M., Mehta, A.D., 2013. Neurophysiological investigation of spontaneous correlated and anticorrelated fluctuations of the bold signal. J. Neurosci. 33 (15), 6333–6342. https://doi.org/10.1523/JNEUROSCI.4837-12.2013.
Kim, P.-J., Kim, H.-G., Noh, G.-J., Koo, Y.-S., Shin, T.J., 2017. Disruption of frontal-parietal connectivity during conscious sedation by propofol administration. Neuroreport 28 (14), 896–902. https://doi.org/10.1097/WNR.0000000000000853.
Larson-Prior, L.J., Zempel, J.M., Nolan, T.S., Prior, F.W., Snyder, A.Z., Raichle, M.E., 2009. Cortical network functional connectivity in the descent to sleep. Proc. Natl. Acad. Sci. U.S.A. 106 (11), 4489–4494. https://doi.org/10.1073/pnas.0900924106.
Lee, H., Mashour, G.A., Noh, G.-J., Kim, S., Lee, U., 2013. Reconfiguration of network hub structure after propofol-induced unconsciousness. Anesthesiology 119 (6), 1347–1359. https://doi.org/10.1097/ALN.0b013e3182a8ec8c.
Lee, J., 2012. Propofol abuse in professionals. J. Korean Med. Sci. 27 (12), 1451–1452. https://doi.org/10.3346/jkms.2012.27.12.1451.
Li, J., Kong, R., Liégeois, R., Orban, C., Tan, Y., Sun, N., Holmes, A.J., Sabuncu, M.R., Ge, T., Yeo, B.T.T., 2019. Global signal regression strengthens association between resting-state functional connectivity and behavior. Neuroimage 196, 126–141.

https://doi.org/10.1016/j.neuroimage.2019.04.016.
Li, K., Liu, L., Yin, Q., Dun, W., Xu, X., Liu, J., Zhang, M., 2017. Abnormal rich club organization and impaired correlation between structural and functional connectivity in migraine sufferers. Brain Imaging Behav. 11 (2), 526–540. https://doi.org/10.1007/s11682-016-9533-6.
Li, Y., Wang, S., Pan, C., Xue, F., Xian, J., Huang, Y., Wang, X., Li, T., He, H., 2018. Comparison of NREM sleep and intravenous sedation through local information processing and whole brain network to explore the mechanism of general anesthesia. PLoS ONE 13 (2), e0192358. https://doi.org/10.1371/journal.pone.0192358.
Liu, X., Lauer, K.K., Ward, B.D., Rao, S.M., Li, S.-J., Hudetz, A.G., 2012. Propofol disrupts functional interactions between sensory and high-order processing of auditory verbal memory. Hum. Brain Mapp. 33 (10), 2487–2498. https://doi.org/10.1002/hbm.21385.
Liu, X., Li, H., Luo, F., Zhang, L., Han, R., Wang, B., 2015. Variation of the default mode network with altered alertness levels induced by propofol. Neuropsychiatr. Dis. Treat. 11, 2573–2581. https://doi.org/10.2147/NDT.S88156.
Liu, X., Li, S.-J., Hudetz, A.G., 2013. Increased precuneus connectivity during propofol sedation. Neurosci. Lett. 561, 18–23. https://doi.org/10.1016/j.neulet.2013.12.047.
Long, J., Xie, Q., Ma, Q., Urbin, M.A., Liu, L., Weng, L., Huang, X., Yu, R., Li, Y., Huang, R., 2016. Distinct interactions between fronto-parietal and default mode networks in impaired consciousness. Sci. Rep. 6, 38866. https://doi.org/10.1038/srep38866.
MacDonald, A.A., Naci, L., MacDonald, P.A., Owen, A.M., 2015. Anesthesia and neuroimaging: investigating the neural correlates of unconsciousness. Trends Cogn. Sci. (Regul. Ed.) 19 (2), 100–107. https://doi.org/10.1016/j.tics.2014.12.005.
Manto, M., Bower, J.M., Conforto, A.B., Delgado-García, J.M., da Guarda, S.N.F, Gerwig, M., Habas, C., Hagura, N., Ivry, R.B., Mariën, P., Molinari, M., Naito, E., Nowak, D.A., Oulad Ben Taib, N., Pelisson, D., Tesche, C.D., Tilikete, C., Timmann, D., 2012. Consensus paper: roles of the cerebellum in motor control–the diversity of ideas on cerebellar involvement in movement. Cerebellum 11 (2), 457–487. https://doi.org/10.1007/s12311-011-0331-9. (London, England).
Marsh, B., White, M., Morton, N., Kenny, G.N., 1991. Pharmacokinetic model driven infusion of propofol in children. Br. J. Anaesth. 67 (1), 41–48. https://doi.org/10.1093/bja/67.1.41.
Mashour, G.A., Hudetz, A.G., 2018. Neural correlates of unconsciousness in large-scale brain networks. Trends Neurosci. 41 (3), 150–160. https://doi.org/10.1016/j.tins.2018.01.003.
Mason, M.F., Norton, M.I., van Horn, J.D., Wegner, D.M., Grafton, S.T., Macrae, C.N., 2007. Wandering minds: the default network and stimulus-independent thought. Science 315 (5810), 393–395. https://doi.org/10.1126/science.1131295. (New York, N.Y.).
Minert, A., Devor, M., 2016. Brainstem node for loss of consciousness due to GABA(A) receptor-active anesthetics. Exp. Neurol. 275 (1), 38–45. https://doi.org/10.1016/j.expneurol.2015.10.001. Pt.
Monti, M.M., Lutkenhoff, E.S., Rubinov, M., Boveroux, P., Vanhaudenhuyse, A., Gosseries, O., Bruno, M.-A., Noirhomme, Q., Boly, M., Laureys, S., 2013. Dynamic change of global and local information processing in propofol-induced loss and recovery of consciousness. PLoS Comput. Biol. 9 (10), e1003271. https://doi.org/10.1371/journal.pcbi.1003271.
Moon, J.-Y., Lee, U., Blain-Moraes, S., Mashour, G.A., 2015. General relationship of global topology, local dynamics, and directionality in large-scale brain networks. PLoS Comput. Biol. 11 (4), e1004225. https://doi.org/10.1371/journal.pcbi.1004225.
Murphy, K., Birn, R.M., Handwerker, D.A., Jones, T.B., Bandettini, P.A., 2008. The impact of global signal regression on resting state correlations: are anti-correlated networks introduced? Neuroimage 44 (3), 893–905. https://doi.org/10.1016/j.neuroimage.2008.09.036.
Murphy, K., Fox, M.D., 2017. Towards a consensus regarding global signal regression for resting state functional connectivity MRI. Neuroimage 154, 169–173. https://doi.org/10.1016/j.neuroimage.2016.11.052.
Namigar, T., Serap, K., Esra, A.T., Özgül, O., Can, Ö., Aysel, A., Achmet, A., 2017. The correlation among the Ramsay sedation scale, Richmond agitation sedation scale and Riker sedation agitation scale during midazolam-remifentanil sedation. Rev. Bras. Anestesiol. 67 (4), 347–354. https://doi.org/10.1016/j.bjan.2017.03.006.
Naro, A., Russo, M., Leo, A., Cannavò, A., Manuli, A., Bramanti, A., Bramanti, P., Calabrò, R.S., 2016. Cortical connectivity modulation induced by cerebellar oscillatory transcranial direct current stimulation in patients with chronic disorders of consciousness: a marker of covert cognition? Clin. Neurophysiol. 127 (3), 1845–1854. https://doi.org/10.1016/j.clinph.2015.12.010.
Niazy, R.K., Xie, J., Miller, K., Beckmann, C.F., Smith, S.M., 2011. Spectral characteristics of resting state networks. Prog. Brain Res. 193, 259–276. https://doi.org/10.1016/B978-0-444-53839-0.00017-X.
Pappas, I., Adapa, R.M., Menon, D.K., Stamatakis, E.A., 2019. Brain network disintegration during sedation is mediated by the complexity of sparsely connected regions. Neuroimage 186, 221–233. https://doi.org/10.1016/j.neuroimage.2018.10.078.
Piece, D.J., 1965. Networks of scientific papers. Science 149 (3683), 510–515 (New York, N.Y.).
Plourde, G., Belin, P., Chartrand, D., Fiset, P., Backman, S.B., Xie, G., Zatorre, R.J., 2006. Cortical processing of complex auditory stimuli during alterations of consciousness with the general anesthetic propofol. Anesthesiology 104 (3), 448–457.
Poerio, G.L., Sormaz, M., Wang, H.-T., Margulies, D., Jefferies, E., Smallwood, J., 2017. The role of the default mode network in component processes underlying the wandering mind. Soc. Cogn. Affect. Neurosci. 12 (7), 1047–1062. https://doi.org/10.1093/scan/nsx041.
Power, J.D., Barnes, K.A., Snyder, A.Z., Schlaggar, B.L., Petersen, S.E., 2012. Spurious but systematic correlations in functional connectivity MRI networks arise from subject motion. Neuroimage 59 (3), 2142–2154. https://doi.org/10.1016/j.neuroimage.2011.10.018.
Purdon, P.L., Pierce, E.T., Bonmassar, G., Walsh, J., Harrell, P.G., Kwo, J., Deschler, D., Barlow, M., Merhar, R.C., Lamus, C., Mullaly, C.M., Sullivan, M., Maginnis, S., Skoniecki, D., Higgins, H.A., Brown, E.N., 2009. Simultaneous electroencephalography and functional magnetic resonance imaging of general anesthesia. Ann. N. Y. Acad. Sci. 1157, 61–70. https://doi.org/10.1111/j.1749-6632.2008.04119.x.
Ramsay, M.A., Savege, T.M., Simpson, B.R., Goodwin, R., 1974. Controlled sedation with alphaxalone-alphadolone. Br. Med. J. 2 (5920), 656–659. https://doi.org/10.1136/bmj.2.5920.656.
Reus, M.A., van den Heuvel, M.P., 2013. Rich club organization and intermodule communication in the cat connectome. J. Neurosci. 33 (32), 12929–12939. https://doi.org/10.1523/JNEUROSCI.1448-13.2013.
Rubinov, M., Sporns, O., 2010. Complex network measures of brain connectivity: uses and interpretations. Neuroimage 52 (3), 1059–1069. https://doi.org/10.1016/j.neuroimage.2009.10.003.
Saad, Z.S., Gotts, S.J., Murphy, K., Chen, G., Jo, H.J., Martin, A., Cox, R.W., 2012. Trouble at rest: how correlation patterns and group differences become distorted after global signal regression. Brain Connect. 2 (1), 25–32. https://doi.org/10.1089/brain.2012.0080.
Satterthwaite, T.D., Elliott, M.A., Gerraty, R.T., Ruparel, K., Loughead, J., Calkins, M.E., Eickhoff, S.B., Hakonarson, H., Gur, R.C., Gur, R.E., Wolf, D.H., 2013. An improved framework for confound regression and filtering for control of motion artifact in the preprocessing of resting-state functional connectivity data. Neuroimage 64, 240–256. https://doi.org/10.1016/j.neuroimage.2012.08.052.
Schölvinck, M.L., Maier, A., Ye, F.Q., Duyn, J.H., Leopold, D.A., 2010. Neural basis of global resting-state fMRI activity. In: Proceedings of the National Academy of Sciences of the United States of America. 107. pp. 10238–10243. https://doi.org/10.1073/pnas.0913110107.
Schroeder, M.P., Weiss, C., Procissi, D., Disterhoft, J.F., Wang, L., 2016. Intrinsic connectivity of neural networks in the awake rabbit. Neuroimage 129, 260–267. https://doi.org/10.1016/j.neuroimage.2016.01.010.
Schröter, M.S., Spoormaker, V.I., Schorer, A., Wohlschläger, A., Czisch, M., Kochs, E.F., Zimmer, C., Hemmer, B., Schneider, G., Jordan, D., Ilg, R., 2012. Spatiotemporal reconfiguration of large-scale brain functional networks during propofol-induced loss of consciousness. J. Neurosci. 32 (37), 12832–12840. https://doi.org/10.1523/JNEUROSCI.6046-11.2012.
Seeley, W.W., Menon, V., Schatzberg, A.F., Keller, J., Glover, G.H., Kenna, H., Reiss, A.L., Greicius, M.D., 2007. Dissociable intrinsic connectivity networks for salience processing and executive control. J. Neurosci. 27 (9), 2349–2356. https://doi.org/10.1523/JNEUROSCI.5587-06.2007.
Shinohe, Y., Higuchi, S., Sasaki, M., Sato, M., Noda, M., Joh, S., Satoh, K., 2016. Changes in brain activation induced by visual stimulus during and after propofol conscious sedation: a functional MRI study. Neuroreport 27 (17), 1256–1260. https://doi.org/10.1097/WNR.0000000000000688.
Short, C.E., Bufalari, A., 1999. Propofol anesthesia. the veterinary clinics of North America. Small Animal Practice 29 (3), 747–778.
Song, X., Yu, B., 2015. Anesthetic effects of propofol in the healthy human brain: functional imaging evidence. J. Anesth. 29 (2), 279–288. https://doi.org/10.1007/s00540-014-1889-4.
Stamatakis, E.A., Adapa, R.M., Absalom, A.R., Menon, D.K., 2010. Changes in resting neural connectivity during propofol sedation. PLoS ONE 5 (12), e14224. https://doi.org/10.1371/journal.pone.0014224.
Thach, W.T., 1998. What is the role of the cerebellum in motor learning and cognition? Trends Cogn. Sci. (Regul. Ed.) 2 (9), 331–337.
Tononi, G., 2004. An information integration theory of consciousness. BMC Neurosci. 5, 42. https://doi.org/10.1186/1471-2202-5-42.
Towlson, E.K., Vértes, P.E., Ahnert, S.E., Schafer, W.R., Bullmore, E.T., 2013. The rich club of the C. elegans neuronal connectome. J. Neurosci. 33 (15), 6380–6387. https://doi.org/10.1523/JNEUROSCI.3784-12.2013.
Uehara, T., Yamasaki, T., Okamoto, T., Koike, T., Kan, S., Miyauchi, S., Kira, J.-I., Tobimatsu, S., 2014. Efficiency of a “small-world” brain network depends on consciousness level: a resting-state FMRI study. Cerebral Cortex 24 (6), 1529–1539. https://doi.org/10.1093/cercor/bht004. (New York, N.Y.: 1991).
Vacas, S., Kurien, P., Maze, M., 2013. Sleep and anesthesia - Common mechanisms of action. Sleep Med. Clin. 8 (1), 1–9. https://doi.org/10.1016/j.jsmc.2012.11.009.
van den Heuvel, M.P., Sporns, O., 2011. Rich-club organization of the human connectome. J. Neurosci. 31 (44), 15775–15786. https://doi.org/10.1523/JNEUROSCI.3539-11.2011.
van den Heuvel, M.P., Sporns, O., 2013. An anatomical substrate for integration among functional networks in human cortex. J. Neurosci. 33 (36), 14489–14500. https://doi.org/10.1523/JNEUROSCI.2128-13.2013.
van Dijk, K.R.A., Sabuncu, M.R., Buckner, R.L., 2012. The influence of head motion on intrinsic functional connectivity MRI. Neuroimage 59 (1), 431–438. https://doi.org/10.1016/j.neuroimage.2011.07.044.
Vértes, P.E., Alexander-Bloch, A., Bullmore, E.T., 2014. Generative models of rich clubs in Hebbian neuronal networks and large-scale human brain networks. Philos. Trans. R. Soc. Lond., B, Biol. Sci. 369 (1653). https://doi.org/10.1098/rstb.2013.0531.
Wang, J., Lu, M., Fan, Y., Wen, X., Zhang, R., Wang, B., Ma, Q., Song, Z., He, Y., Wang, J., Huang, R., 2016. Exploring brain functional plasticity in world class gymnasts: a network analysis. Brain Struct. Funct. 221 (7), 3503–3519. https://doi.org/10.1007/s00429-015-1116-6.
Wang, J., Wang, X., Xia, M., Liao, X., Evans, A., He, Y., 2015. GRETNA: a graph theoretical network analysis toolbox for imaging connectomics. Front. Hum. Neurosci. 9. https://doi.org/10.3389/fnhum.2015.00386.
Watts, D.J., Strogatz, S.H., 1998. Collective dynamics of ‘small-world’ networks. Nature 393 (6684), 440–442. https://doi.org/10.1038/30918.

Wen, H., Liu, Y., Rekik, I., Wang, S., Zhang, J., Zhang, Y., Peng, Y., He, H., 2017. Disrupted topological organization of structural networks revealed by probabilistic diffusion tractography in Tourette syndrome children. Hum. Brain Mapp. 38 (8), 3988–4008. https://doi.org/10.1002/hbm.23643.

Wong, C.W., Olafsson, V., Tal, O., Liu, T.T., 2013. The amplitude of the resting-state fMRI global signal is related to EEG vigilance measures. Neuroimage 83, 983–990. https://doi.org/10.1016/j.neuroimage.2013.07.057.

Xia, M., Wang, J., He, Y., 2013. BrainNet viewer: a network visualization tool for human brain connectomics. PLoS ONE 8 (7). https://doi.org/10.1371/journal.pone.0068910.

Xu, H., Su, J., Qin, J., Li, M., Zeng, L.-L., Hu, D., Shen, H., 2018. Impact of global signal regression on characterizing dynamic functional connectivity and brain states. Neuroimage 173, 127–145. https://doi.org/10.1016/j.neuroimage.2018.02.036.

Xu, X.-K., Zhang, J., Small, M., 2010. Rich-club connectivity dominates assortativity and transitivity of complex networks. Phys. Rev. E Stat. Nonlin. Soft Matter Phys. 82 (4 Pt 2), 46117. https://doi.org/10.1103/PhysRevE.82.046117.

Yan, C.-G., Cheung, B., Kelly, C., Colcombe, S., Craddock, R.C., Di Martino, A., Li, Q., Zuo, X.-N., Castellanos, F.X., Milham, M.P., 2013. A comprehensive assessment of regional variation in the impact of head micromovements on functional connectomics. Neuroimage 76, 183–201. https://doi.org/10.1016/j.neuroimage.2013.03.004.

Yan, C.-G., Wang, X.-D., Zuo, X.-N., Zang, Y.-F., 2016. DPABI: data processing & analysis for (Resting-State) brain imaging. Neuroinformatics 14 (3), 339–351. https://doi.org/10.1007/s12021-016-9299-4.

Yang, Z., Craddock, R.C., Margulies, D., Yan, C.-G., Milham, M.P., 2014. Common intrinsic connectivity states among posteromedial cortex subdivisions: insights from analysis of temporal dynamics. Neuroimage 93 (0 1), 124–137. https://doi.org/10.1016/j.neuroimage.2014.02.014.

Yao, Z., Hu, B., Xie, Y., Moore, P., Zheng, J., 2015. A review of structural and functional brain networks: small world and atlas. Brain Informat. 2 (1), 45–52. https://doi.org/10.1007/s40708-015-0009-z.

Yin, P., Zhang, M., Hou, X., Tan, Y., Fu, Y., Qiu, J., 2016. The brain structure and spontaneous activity baseline of the behavioral bias in trait anxiety. Behav. Brain Res. 312, 355–361. https://doi.org/10.1016/j.bbr.2016.06.036.

Zalucki, O., van Swinderen, B., 2016. What is unconsciousness in a fly or a worm? A review of general anesthesia in different animal models. Conscious. Cogn. 44, 72–88. https://doi.org/10.1016/j.concog.2016.06.017.

Zecharia, A.Y., Nelson, L.E., Gent, T.C., Schumacher, M., Jurd, R., Rudolph, U., Brickley, S.G., Maze, M., Franks, N.P., 2009. The involvement of hypothalamic sleep pathways in general anesthesia: testing the hypothesis using the GABAA receptor beta3N265M knock-in mouse. J. Neurosci. 29 (7), 2177–2187. https://doi.org/10.1523/JNEUROSCI.4997-08.2009.

Zhao, X., Tian, L., Yan, J., Yue, W., Yan, H., Zhang, D., 2017. Abnormal rich-club organization associated with compromised cognitive function in patients with schizophrenia and their unaffected parents. Neurosci. Bull. 33 (4), 445–454. https://doi.org/10.1007/s12264-017-0151-0.